

# Kicked-Harper model vs On-Resonance Double Kicked Rotor Model: From Spectral Difference to Topological Equivalence

Hailong Wang,<sup>1</sup> Derek Y. H. Ho,<sup>1</sup> Wayne Lawton,<sup>2</sup> Jiao Wang,<sup>3,\*</sup> and Jiangbin Gong<sup>1,4,†</sup>

<sup>1</sup>*Department of Physics and Center for Computational Science and Engineering,  
National University of Singapore, 117542, Singapore*

<sup>2</sup>*School of Mathematics and Statistics,  
University of Western Australia, Perth, Australia*

<sup>3</sup>*Department of Physics and Institute of Theoretical Physics and Astrophysics,  
Xiamen University, Xiamen 361005, China*

<sup>4</sup>*NUS Graduate School for Integrative Sciences  
and Engineering, Singapore 117597, Singapore*

(Dated: November 19, 2018)

## Abstract

Recent studies have established that, in addition to the well-known kicked Harper model (KHM), an on-resonance double kicked rotor model (ORDKR) also has Hofstadter's butterfly Floquet spectrum, with strong resemblance to the standard Hofstadter's spectrum that is a paradigm in studies of the integer quantum Hall effect. Earlier it was shown that the quasi-energy spectra of these two dynamical models (i) can exactly overlap with each other if an effective Planck constant takes irrational multiples of  $2\pi$  and (ii) will be different if the same parameter takes rational multiples of  $2\pi$ . This work makes some detailed comparisons between these two models, with an effective Planck constant given by  $2\pi M/N$ , where  $M$  and  $N$  are coprime and odd integers. It is found that the ORDKR spectrum (with two periodic kicking sequences having the same kick strength) has one flat band and  $N - 1$  non-flat bands whose largest width decays in power law as  $\sim K^{N+2}$ , where  $K$  is a kicking strength parameter. The existence of a flat band is strictly proven and the power law scaling, numerically checked for a number of cases, is also analytically proven for a three-band case. By contrast, the KHM does not have any flat band and its band width scales linearly with  $K$ . This is shown to result in dramatic differences in dynamical behavior, such as transient (but extremely long) dynamical localization in ORDKR, which is absent in KHM. Finally, we show that despite these differences, there exist simple extensions of KHM and ORDKR (upon introducing an additional periodic phase parameter) such that the resulting extended KHM and ORDKR are actually topologically equivalent, i.e., they yield exactly the same Floquet-band Chern numbers and display topological phase transitions at the same kick strengths. A theoretical derivation of this topological equivalence is provided. These results are also of interest to our current understanding of quantum-classical correspondence considering that KHM and ORDKR have exactly the same classical limit after a simple canonical transformation.

PACS numbers: 05.45.Df, 05.45.Mt, 71.30.+h, 74.40.Kb, 05.45.-a

---

\*Electronic address: phywangj@xmu.edu.cn

†Electronic address: phygj@nus.edu.sg

## I. INTRODUCTION

As one important paradigm in the studies of quantum chaos and quantum-classical correspondence, the kicked rotor (KR) model [1] has received tremendous theoretical and experimental interest in the last three decades [1, 2]. For some experimental activities on KR within the last three years, we would like to mention those listed in Ref. [3]. A one-dimensional KR is described by the Hamiltonian

$$H_{\text{KR}} = p^2/2 + K \cos(q) \sum_n \delta(t - nT) \quad (1)$$

in terms of dimensionless variables, where  $p$  and  $q$  are conjugate (angular) momentum and angle variables,  $K$  and  $T$  are the kick strength and the period of the  $\delta$ -kicks. The dynamical evolution of the system for a period from time  $nT + 0^-$  to  $(n + 1)T + 0^-$  can be expressed as a quantum map, which is given by the following unitary Floquet operator

$$U_{\text{KR}} = e^{-iT\frac{p^2}{2\hbar}} e^{-i\frac{K}{\hbar} \cos(q)}. \quad (2)$$

For our considerations below, we confine ourselves to a rotor Hilbert space defined by the periodic boundary condition in  $q$ , with  $q \in [0, 2\pi)$ . The Hilbert space can then be represented by the eigenfunctions  $\{|m\rangle\}$  of  $p$ , with  $p|m\rangle = m\hbar|m\rangle$ ,  $\langle q|m\rangle = \exp(imq)/\sqrt{2\pi}$ ,  $m$  being an integer, and  $\hbar$  being a dimensionless effective Planck constant. Through extensive numerical simulations and mathematical analysis, it is now well known that in general the KR dynamics can be classified into two categories [2]. For an irrational (hence generic) value of  $T\hbar/(2\pi)$  the system can diffuse in (angular) momentum space only for a short time due to “dynamical localization”, regardless of the kick strength. This hints at a discrete spectrum of  $U_{\text{KR}}$  and is closely related to Anderson localization [4]. On the other hand, for  $T\hbar/(2\pi)$  being a rational multiple of  $2\pi$  (except for odd multiples of  $2\pi$ ),  $U_{\text{KR}}$  has continuous bands: A time-evolving state would keep spreading out in (angular) momentum space ballistically. This category of dynamics was termed as “quantum resonance” [5].

Another important quantum chaos model is the kicked Harper model (KHM) [6–8], originally introduced in Ref. [9] as an approximation of the problem of kicked charges in a magnetic field. Remarkably, the KHM and even a whole class of its generalized versions were shown to be equivalent to the problem of a charge kicked periodically in the presence of a magnetic field [10]. The associated KHM quantum map for each period is given by

$$U_{\text{KHM}} = e^{-i\frac{L}{\hbar} \cos(p)} e^{-i\frac{K}{\hbar} \cos(q)}, \quad (3)$$

with  $L$  being an additional system parameter. Throughout we assume the KHM is also treated in the same Hilbert space as the KR and is quantized on a rotor Hilbert space. The dynamics of KHM differs from that of KR as described above in several aspects. For example, for all irrational values of  $\hbar/(2\pi)$ , the system in general tends to delocalize (localize) in (angular) momentum space for  $K > L$  ( $K < L$ ) [8]. Of particular interest is the symmetric case of  $K = L$ , for which the quasi-energy spectrum of  $U_{\text{KHM}}$  is fractal-like in general. Scanning the spectrum collectively for fixed  $K/\hbar = L/\hbar$  versus a varying  $\hbar$  forms a pattern that resembles the Hofstadter's butterfly spectrum [11], a paradigm in studies of the integer quantum Hall effect. The associated dynamics is extended in general and may be connected with the fractal dimensions of the Floquet spectrum.

Given the above-mentioned differences between KR and KHM, the work of Ref. [12] by two of the authors emerged somewhat unexpectedly. There it was shown that a variant of KR also has Hofstadter's butterfly spectrum. In particular, motivated by the double-kicked rotor model studied both experimentally and theoretically in Ref. [13], which is a special case of "multiple KR's" first introduced in Ref. [14], Ref. [12] studied a double-kicked model under a quantum-resonance condition. For a total period of  $\tau$  ( $\tau > 1$ ), a double kicked rotor model is associated with two periodic  $\delta$ -kicks of strengths  $K$  and  $L$ , separated by a time interval set to be unity, yielding the following Floquet operator

$$U_{\text{DKR}} = e^{-i(\tau-1)\frac{p^2}{2\hbar}} e^{-i\frac{K}{\hbar} \cos(q)} e^{-i\frac{p^2}{2\hbar}} e^{-i\frac{L}{\hbar} \cos(q)}. \quad (4)$$

In Ref. [12],  $\tau$  is chosen to satisfy the quantum resonance condition  $\tau\hbar = 4\pi$ . Then  $e^{-i\tau\frac{p^2}{2\hbar}} = 1$  due to the discreteness of the momentum eigenvalues. This leads us to an on-resonance double kicked rotor model (ORDKR), whose Floquet operator is given by [15]:

$$U_{\text{ORDKR}} = e^{i\frac{p^2}{2\hbar}} e^{-i\frac{K}{\hbar} \cos(q)} e^{-i\frac{p^2}{2\hbar}} e^{-i\frac{L}{\hbar} \cos(q)}. \quad (5)$$

Note that we have deliberately used symbols  $K$  and  $L$  in both  $U_{\text{KHM}}$  and  $U_{\text{ORDKR}}$  because in this paper, parameter  $K$  or parameter  $L$  from both models will always be assigned the same value. Experimental realization of such an ORDKR propagator in atom optics is possible by loading a Bose-Einstein-Condensate (BEC) in a kicking optical lattice, with the initial quasi-momentum spread of the BEC negligibly small as compared with the recoil momentum of the optical lattice [16]. Interestingly, for  $\hbar$  being an irrational multiple of  $2\pi$ , the ORDKR and the KHM share the same quasi-energy spectrum [17, 18].

Our main plan for this paper is to make some detailed comparisons between KHM and ORDKR as two closely related dynamical models, both possessing Hofstadter’s butterfly spectrum. Our motivations are as follows. First of all, in Refs. [12, 17], it was shown that  $U_{\text{ORDKR}}$  and  $U_{\text{KHM}}$  have different spectra if  $\hbar$  is a rational multiple of  $2\pi$ . On the other hand, as  $\hbar/(2\pi)$  approaches an arbitrary irrational number, the spectral difference between  $U_{\text{ORDKR}}$  and  $U_{\text{KHM}}$ , which is characterized by a Hausdorff metric in Ref. [17], was shown to approach zero. It is therefore highly worthwhile looking into the actual spectral differences for rational values of  $\hbar/(2\pi)$ , because, up to a classical canonical transformation, ORDKR and KHM have exactly the same classical limit [19] (obtained by letting  $\hbar$  approach zero while fixing  $K/\hbar$  and  $L/\hbar$ ). Indeed, given their equivalence in the classical limit, the spectral differences we analyze constitute beautiful examples to illustrate how quantization of classically equivalent systems may lead to remarkable system-specific consequences. Second, by working on the details we hope to find some clues as to why the dynamics of ORDKR can be so different from that of KHM. We indeed succeed in doing this, finding that even on a qualitative level, the Floquet bands of ORDKR behave much differently from that of KHM, for  $\hbar = 2\pi M/N$ , with  $M$  and  $N$  being coprime and both odd. In particular, we shall prove the existence of a flat Floquet band [14, 20] for ORDKR with  $K = L$ , which may be of interest to current studies of strongly correlated condensed-matter systems with an almost flat energy band [21]. The existence of a flat Floquet band has been shown elsewhere to be important in explaining the intriguing exponential quantum spreading dynamics in ORDKR [22, 23]. Third, motivated by recent interests in topological characterization of periodically driven systems [24, 25] and given the interesting relationship of the two models described previously, we ask whether, after all, ORDKR and KHM have any interesting topological connections. Based on our numerical and analytical studies, the answer is yes and we shall claim that ORDKR and KHM are topologically equivalent in the sense that their extended Floquet bands (obtained upon introducing a phase shift parameter defined in Sec. III) always have the same band Chern numbers.

This paper is organized in the following order. In Sec. II we present detailed results regarding a spectral comparison between KHM and ORDKR, for  $K = L$ , and  $\hbar = 2\pi M/N$  with  $M$  and  $N$  being coprime and odd integers. Numerical findings will be described first, followed by analytical considerations when possible (e.g., band width scaling for a three-band case and the general proof of a flat band for ORDKR). The implications of peculiar spectral

properties of ORDKR for its dynamics are also discussed via some numerical studies. In Sec. III we study the KHM and ORDKR by extending them to accommodate a new periodic parameter and demonstrating the topological equivalence of the resulting extended models. Section IV concludes this paper.

## II. SPECTRAL DIFFERENCES AND THEIR DYNAMICAL IMPLICATIONS

### A. Summary of main numerical findings

As far as numerics are concerned, the spectrum of the unitary operators can be obtained in a straightforward manner. For completeness we describe some details here. The key step is to take advantage of the periodic property of  $U_{\text{KHM}}$  or  $U_{\text{ORDKR}}$  in the (angular) momentum space, which arises naturally for  $\hbar$  being a rational multiple of  $2\pi$ . Denote  $U$  to refer to either  $U_{\text{KHM}}$  or  $U_{\text{ORDKR}}$ . Letting  $U_{j,k} \equiv \langle j|U|k\rangle$ , one easily finds  $U_{j+N,k+N} = U_{j,k}$  for  $\hbar = 2\pi M/N$ . This indicates a unit cell in (angular) momentum space, with a size of  $N$ . The spectrum is then equivalent to that of a reduced  $N \times N$  matrix  $\tilde{U}(\varphi)$ , whose elements are given by  $[\tilde{U}(\varphi)]_{j,k} = \sum_l e^{il\varphi} U_{j,k+lN}$ , with  $\varphi \in [0, 2\pi)$  being the Bloch phase in momentum space and  $l$  running over all integers. As off-diagonal elements of  $U_{j,k}$  decay exponentially, the summation in  $\sum_l e^{il\varphi} U_{j,k+lN}$  can be truncated safely at certain large enough value of  $|l|$  (in our analytical studies below, we do not do such truncations). Numerical results are then checked by further increasing the truncation radius. Once  $\tilde{U}(\varphi)$  is numerically obtained, the standard diagonalization algorithm for a unitary matrix can be exploited to obtain  $N$  values of quasi-energy  $\epsilon$ . By varying  $\varphi$  in  $[0, 2\pi)$  we have  $N$  Floquet bands.

In Fig. 1 we show our obtained quasi-energy values of  $U_{\text{ORDKR}}$  and  $U_{\text{KHM}}$  as a function of the kick strength  $K$ . Though for each fixed value of  $K$ , we only show the quasi-energy values for a limited number of Bloch phase choices, the locations of the bands, the band width, and a few avoided band crossings can already be seen clearly for not too large values of  $K = L$ . In particular, at  $N = 9$ , nice Floquet bands can be identified clearly for both ORDKR and KHM, though for very large values of  $K$  the merging of the bands does occur.

Spectral differences between  $U_{\text{ORDKR}}$  and  $U_{\text{KHM}}$  in the shown example are also obvious. Based on the results shown in Fig. 1, we have carried out extensive numerical investigations for other cases with  $\hbar = 2\pi M/N$ , with  $M$  and  $N$  coprime and both odd. Some of the main

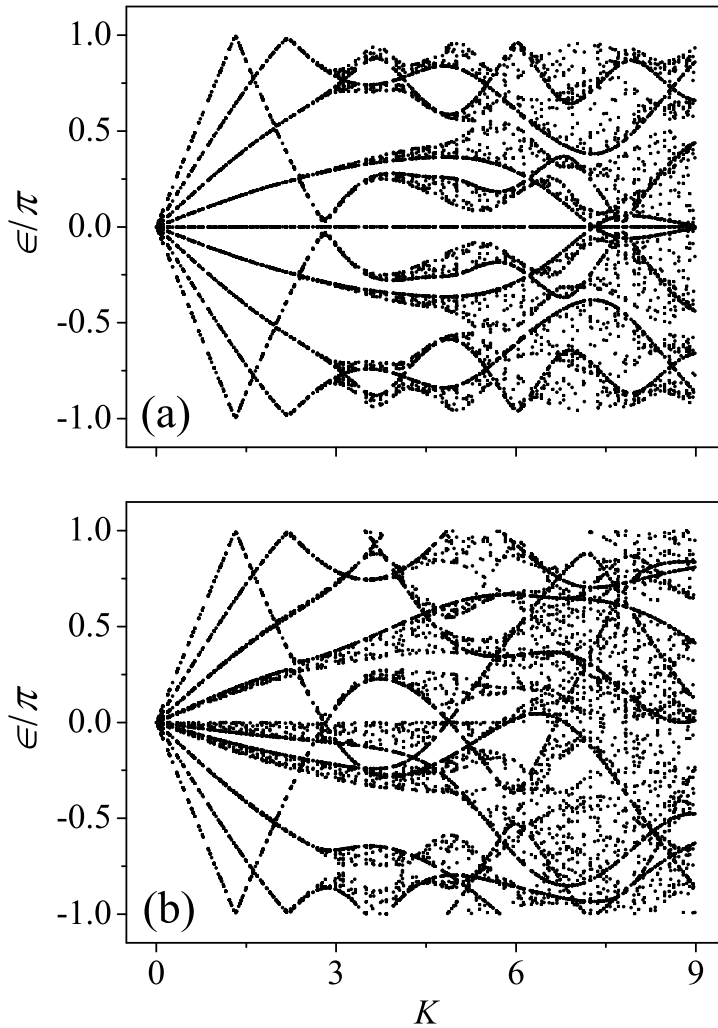


FIG. 1: The quasi-energy bands versus the kick strength  $K = L$  for an effective Planck constant  $\hbar = 2\pi M/N$ , with  $M = 1$  and  $N = 9$ , for ORDKR in panel (a) for KHM in panel (b). Note that for ORDKR, there is a straight line lying in the middle of the spectrum, indicating the existence of a flat band. Here and in all other figures, all plotted quantities are in dimensionless units.

features are presented and commented on below.

First, the band structure of  $U_{\text{ORDKR}}$  is symmetric with respect to the zero quasi-energy axis, which is however not the case for  $U_{\text{KHM}}$ . This interesting symmetry is absent in both  $U_{\text{KHM}}$  and  $U_{\text{KR}}$ . We shall prove this property below.

Second, consistent with the above-mentioned symmetry,  $U_{\text{ORDKR}}$  is seen to have a flat band with  $\epsilon = 0$ . By flat band, we mean that this quasi-energy value is independent

of the Bloch phase  $\varphi$ . So the overall picture is that the  $N$  bands can be classified into  $(N - 1)/2$  pairs, with each pair having opposite quasi-energy values, plus a flat band in the middle. Again, this is not the case for  $U_{\text{KHM}}$ . The existence of a flat Floquet band was previously observed in studies of the quantum antiresonance phenomenon in kicked systems [14, 20]. However, unless in the case of  $N = 1$  ( $M$  odd) that also corresponds to a quantum antiresonance condition, here the flat band of  $U_{\text{ORDKR}}$  coexists with other nonflat bands. This coexistence of a flat band with nonflat bands constitutes an interesting feature. As a side note, Ref. [26] suggested that for a KR defined in this paper under the quantum resonance condition of any order (i.e.,  $T\hbar = 4\pi M/N$ , with  $M$  and  $N$  arbitrary coprime integers), none of the Floquet bands of  $U_{\text{KR}}$  is flat. So the existence of one single flat band of  $U_{\text{ORDKR}}$  is also remarkable as compared with  $U_{\text{KR}}$ .

Third, the largest bandwidth of the other  $N - 1$  non-flat Floquet bands of ORDKR scales with  $K$  as  $\sim K^{N+2}$ , in the limit of  $K \rightarrow 0$ . In sharp contrast, the bandwidths of KHM scale with  $K$  linearly. Representative numerical results are shown in Fig. 2, where the bandwidth of the widest band is plotted against small values of  $K$ , for  $\hbar = 2\pi M/N$ , with  $M = 1, N = 3, 5, 7, 9$ . The power law decay of the ORDKR bandwidth in the form of  $\sim K^{N+2}$  can be clearly identified, whereas the bandwidth of KHM remains a linear function of  $K$ , irrespective of the value of  $N$ . This being the case, in the small  $K$  regime ( $K \ll 1$ ), the maximum bandwidths of ORDKR is  $K^{N+1}$  times narrower than that of KHM.

## B. Flat band and Band symmetry in ORDKR

Flat bands in solid-state systems are of vast interest in condensed matter physics because they offer new opportunities for understanding strongly correlated systems without Landau levels. For this reason the existence of a flat band in a periodically driven system can be useful, too. To further understand the flat band of ORDKR, we present a theoretical proof in this subsection. In doing so we shall also prove the band symmetry noted above. We shall also discuss how an eigenstate on a flat band, which is infinitely degenerate, may be numerically found.

For  $\hbar = 2\pi M/N$  with  $M$  and  $N$  being coprime integers, the spectrum becomes that of a reduced  $N \times N$  Floquet matrix with elements  $[\tilde{U}_{\text{ORDKR}}(\varphi)]_{n,m} = \sum_{l=-\infty}^{\infty} \langle n | \hat{U}_{\text{ORDKR}} | m + l \times N \rangle e^{il\varphi}$ . After performing some necessary integrals and using



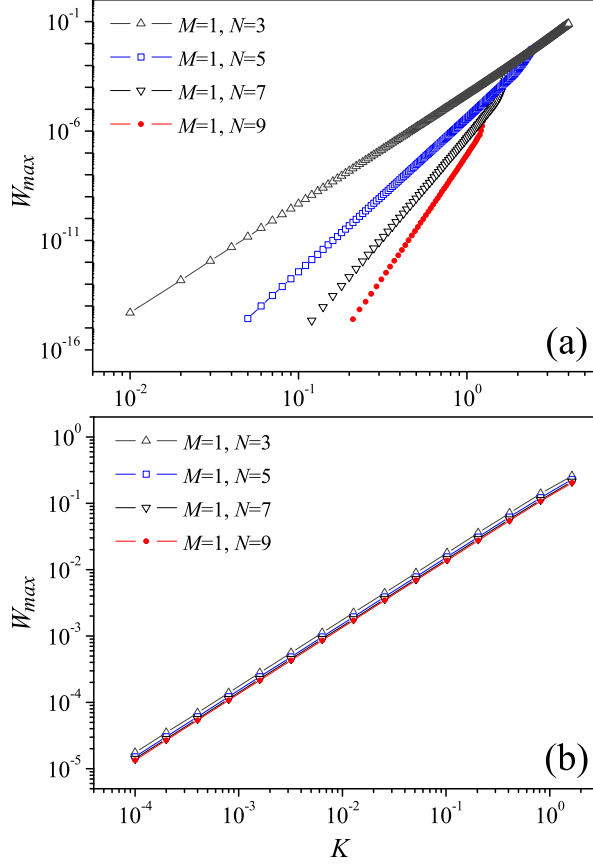


FIG. 2: (color online) The bandwidth of the widest band, denoted  $W_{max}$ , as a function of the kick strength parameter  $K = L$  for (a) ORDKR and (b) KHM. In both panels, the effective Planck constant  $\hbar = 2\pi M/N$  with  $M = 1$  and  $N = 3, 5, 7$ , and  $9$ , respectively. In the former case  $W_{max} \sim K^{N+2}$  as  $K \rightarrow 0$  but in the latter case it always scales linearly with  $K$ .

the fact that both  $M$  and  $N$  are odd, one can express  $\left[\tilde{U}_{\text{ORDKR}}(\varphi)\right]_{n,m}$  as a summation of finite terms (see Appendix for details). In the following discussions regarding the existence of a flat band and the band inversion symmetry, we shall restrict ourselves to the cases of  $K = L$  (note however, in the next section, the notation introduced here will be extended to the cases with  $K \neq L$ ). We first introduce diagonal unitary matrices  $D_\varphi$ ,  $D_1$ ,  $D_K$  and unitary matrix  $F$ , with matrix elements  $(D_\varphi)_{n,m} = e^{-in\frac{\varphi}{N}}\delta_{n,m}$ ,  $(D_1)_{n,m} = e^{i\frac{2\pi-\hbar}{2}n^2}\delta_{n,m}$ ,  $(D_K)_{n,m} = e^{-i\frac{K}{\hbar}\cos(\frac{2\pi}{N}n-\frac{\varphi}{N})}\delta_{n,m}$  and  $F_{m,n} = \frac{1}{\sqrt{N}}e^{i\frac{2\pi}{N}mn}$ , where indices  $m$  and  $n$  take values  $0, 1, \dots, N-1$ . Note that in obtaining our expression for  $D_1$ , we made use of the fact that  $e^{in2\pi} = e^{in\pi}$ . We then have the following compact form for the reduced Floquet matrix

$$\tilde{U}_{\text{ORDKR}}(\varphi) = D_\varphi^\dagger D_1^\dagger F^\dagger D_K^\dagger F D_1 F^\dagger D_K F D_\varphi. \quad (6)$$

To prove that there is a flat band for ORDKR, we show that  $\tilde{U}_{\text{ORDKR}}(\varphi)$  has an eigenvalue equal to one, regardless of the value of  $\varphi$ . Consider then a matrix  $\tilde{U}'_{\text{ORDKR}}(\varphi)$  transformed from  $\tilde{U}_{\text{ORDKR}}(\varphi)$  by a unitary operation  $FD_\varphi$ , which takes the form

$$\tilde{U}'_{\text{ORDKR}}(\varphi) = \left( FD_1^\dagger F^\dagger \right) D_K^\dagger \left( FD_1 F^\dagger \right) D_K. \quad (7)$$

The eigenvalue equation of  $\tilde{U}'_{\text{ORDKR}}(\varphi)$  may be rewritten as

$$(BD_K - \lambda D_K B)|x\rangle = 0, \quad (8)$$

where  $B \equiv FD_1 F^\dagger$ ,  $|x\rangle$  denotes an eigenvector, and  $\lambda$  is an eigenvalue of  $\tilde{U}_{\text{ORDKR}}(\varphi)$ . Detailed calculations show that  $B$  is a symmetric matrix (see Appendix for details) and since  $D_K$  is a diagonal matrix,  $(BD_K - D_K B)$  must be an antisymmetric matrix of odd dimension. It immediately follows  $\text{Det}(BD_K - D_K B) = 0$ . Thus, regardless of the Bloch phase  $\varphi$ ,  $\lambda = 1$  is a permissible solution to Eq. (8). We have thus shown that  $\tilde{U}_{\text{ORDKR}}(\varphi)$  always has a unity eigenvalue or zero quasi-energy for  $\hbar = 2\pi M/N$ . This is nothing but the existence of a flat Floquet band.

Our considerations above also lead us to a proof of the band inversion symmetry of ORDKR for odd  $M$  and  $N$ . Specifically, because  $(BD_K - \lambda D_K B)^T = (D_K B - \lambda B D_K) = -\lambda(BD_K - \lambda^{-1} D_K B)$ , we see that if  $\text{Det}(BD_K - \lambda D_K B) = 0$ , then  $\text{Det}(BD_K - \lambda^{-1} D_K B) = 0$  as well. That is, both  $\lambda$  and  $\lambda^{-1}$  are solutions to the eigenvalue equation of Eq. (8). As such, if we have a quasi-energy  $\epsilon = i \ln \lambda$ , we must have  $i \ln \lambda^{-1} = -\epsilon$  in the spectrum. This completes our proof of the inversion symmetry of the ORDKR.

A flat band is infinitely degenerate as states on the band can still have a continuous Bloch phase  $\varphi$ . Due to such an independence upon the Bloch phase, the band dispersion relation directly yields a zero group velocity in the (angular) momentum space, thus indicating a zero mobility in the (angular) momentum space. Further, the infinite degeneracy allows us to construct a flat-band eigenstate that is localized in the (angular) momentum space (though the Floquet operator itself is periodic in momentum with a period  $N\hbar$ ). It is interesting to outline a simple approach to the construction of flat-band states. It is found that, highly localized flat-band states can be obtained by directly truncating the full Floquet matrix  $U_{\text{ORDKR}}(\varphi)$  to a small size, such that there is only one eigenstate whose eigenvalue is real and still equals to unity (thus not affected by the truncation). Other localized states on the flat band can be obtained by shifting it by a multiple of  $N$  sites, or by superimposing these

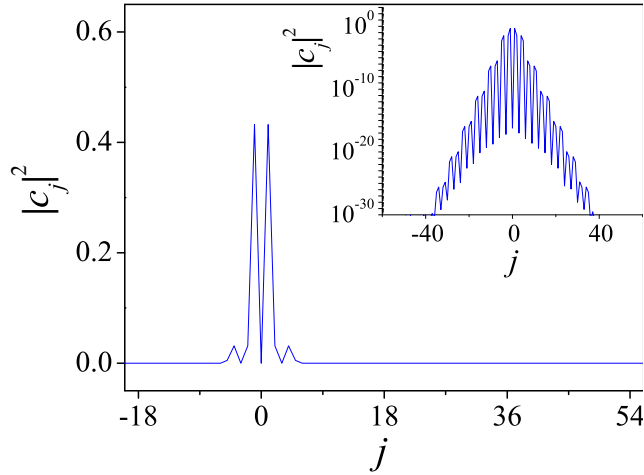


FIG. 3: (color online) A localized eigenstate  $|\psi\rangle = \sum_j c_j |j\rangle$  associated with the flat-band in the on-resonance double kicked rotor model for  $K = 3$  and  $\hbar = 2\pi/3$ . The insert is the same but in semi-log scale.

states localized at different locations. Figure 3 depicts one computational example of a flat-band eigenstate strongly localized in the (angular) momentum space. We have checked that if we use a flat-band state we constructed as the initial state for time evolution, then indeed this state does not evolve with iterations of our ORDKR quantum map. This situation is more subtle than the quantum antiresonance phenomenon [14, 20]: for ORDKR with multiple bands, only special states prepared on the single flat band can remain localized, whereas in the case of quantum antiresonance an arbitrary state should remain localized.

### C. A theoretical bandwidth result and its dynamical consequence

For  $\hbar = 2\pi M/N$  with  $M$  and  $N$  being coprime integers, the reduced  $N \times N$  Floquet matrices  $\tilde{U}_{\text{ORDKR}}(\varphi)$  and  $\tilde{U}_{\text{KHM}}(\varphi)$  (see our general expressions in the Appendix) can be obtained analytically. To further understand and confirm the bandwidth scaling of ORDKR and KHM, we have also carried out analytical studies for a three-band case, with  $K = L$  and  $\hbar = 2\pi/3$ .

For ORDKR, the three eigenvalues are found to be 1 and  $e^{\pm i\epsilon(\varphi)}$ , where  $\epsilon(\varphi) \equiv \arccos[\frac{1}{2}\text{Tr}\tilde{U}(\varphi) - \frac{1}{2}]$ . One finally finds  $\epsilon(\varphi) = \arccos\{\frac{1}{3}[2\cos(\frac{\sqrt{3}K}{2\hbar}\sin\frac{\varphi}{3})\cos(\frac{3K}{2\hbar}\cos\frac{\varphi}{3}) +$

$\cos(\frac{\sqrt{3}K}{h} \sin \frac{\varphi}{3})\}}\}$  where  $\hbar = \frac{2\pi}{3}$ . For  $K < 1$  it can be shown that the edges of the band correspond to  $\varphi = 0(\pi)$  and  $\varphi = \frac{\pi}{2}(\frac{3\pi}{2})$ . The bandwidth can thus be determined to be  $\arccos\left\{\left[\cos(\frac{\sqrt{3}K}{h}) + 2\cos(\frac{\sqrt{3}K}{2h})\right]/3\right\} - \arccos\left[\frac{1}{3} + \frac{2}{3}\cos\left(\frac{3K}{2h}\right)\right]$ . Taylor expanding this expression for the bandwidth, we find the first nonzero term to be  $\frac{\sqrt{6}}{1280}(\frac{K}{h})^5$ , a clear power-law scaling of  $K^5$ .

For KHM, the eigenvalues can be deduced from the equation  $\text{Det}\left(\tilde{U}_{\text{KHM}}(\varphi) - \lambda\right) = 0$ . The resulting explicit expression of the eigenvalue equation is

$$\lambda^3 - 3re^{i\theta}\lambda^2 + 3re^{-i\theta}\lambda - 1 = 0, \quad (9)$$

where  $re^{i\theta} = \frac{1}{9}\left(e^{-i\frac{K}{h}} + 2e^{i\frac{K}{2h}}\right)\left(e^{-i\frac{K}{h}\cos\frac{\varphi}{3}} + 2e^{i\frac{K}{2h}\cos\frac{\varphi}{3}}\cos(\frac{\sqrt{3}K}{2h}\sin\frac{\varphi}{3})\right)$ . Note that all eigenvalues are in the form of  $\lambda \equiv e^{-i\epsilon}$ , since the reduced Floquet matrix is always unitary. The three eigenvalues are found to be  $e^{-i\epsilon_1} = re^{i\theta} + (re^{2i\theta} - e^{-i\theta})\frac{r}{z} + z$ ,  $e^{-i\epsilon_2} = re^{i\theta} + e^{-\frac{2i\pi}{3}}(re^{2i\theta} - e^{-i\theta})\frac{r}{z} + e^{\frac{2i\pi}{3}}z$  and  $e^{-i\epsilon_3} = re^{i\theta} + e^{\frac{2i\pi}{3}}(re^{2i\theta} - e^{-i\theta})\frac{r}{z} + e^{-\frac{2i\pi}{3}}z$  where  $z = \left(\frac{1}{2} - \frac{3}{2}r^2 + r^3e^{3i\theta} + \sqrt{\frac{1}{4} - \frac{3}{2}r^2 + 2r^3\cos(3\theta) - \frac{3}{4}r^4}\right)^{\frac{1}{3}}$ . For  $K < 1$ , the edges of the band correspond to  $\varphi = 0$  and  $\varphi = \pi$ . The band width can thus be determined to be  $W_1 = |\epsilon_1(\varphi = 0) - \epsilon_1(\varphi = \pi)|$ ,  $W_2 = |\epsilon_2(\varphi = 0) - \epsilon_2(\varphi = \pi)|$  and  $W_3 = |\epsilon_3(\varphi = 0) - \epsilon_3(\varphi = \pi)|$ . Taylor expanding the expressions of eigenvalues for  $K \ll 1$  and keeping the lowest order in  $K$ , we have  $W_1 \approx \sqrt{2}\sin(\frac{\pi}{12})\frac{K}{h}$ ,  $W_2 \approx \left(\sqrt{\frac{3}{2}} - 1\right)\frac{K}{h}$  and  $W_3 \approx \left(\sqrt{2}\cos(\frac{\pi}{12}) - \sqrt{\frac{3}{2}}\right)\frac{K}{h}$ , a clear linear scaling of  $K$ .

The very fast decay of the Floquet bandwidth of ORDKR suggests that in a considerable range of  $K$  the bandwidths will be very narrow. In other words, for a small  $K$ , all the Floquet bandwidths would be effectively zero for a reasonably long time scale. Therefore, when it comes to the dynamical evolution of the system, effectively the system will not feel its continuous Floquet spectrum and hence displays localization behavior, for a time scale inversely proportional to the bandwidths. We call this the time scale of transient dynamical localization and denote it by  $T_{\text{tr}}$ . We then have  $T_{\text{tr}} \sim K^{-(N+2)}$ . The overall expectation is the following: within  $T_{\text{tr}}$ , ORDKR displays localization in the (angular) momentum space, but afterwards it begins to show ballistic behavior in the (angular) momentum space. Because of the power law scaling, the intriguing time scale  $T_{\text{tr}}$  can be very sensitive to a change in the kick strength  $K$ . Our numerical calculations indeed confirm this. Figure 4(a) shows an example of the dynamics of the kinetic energy of ORDKR, starting from an initial state with zero momentum. In all three of the shown cases, the kinetic energy is seen to freeze

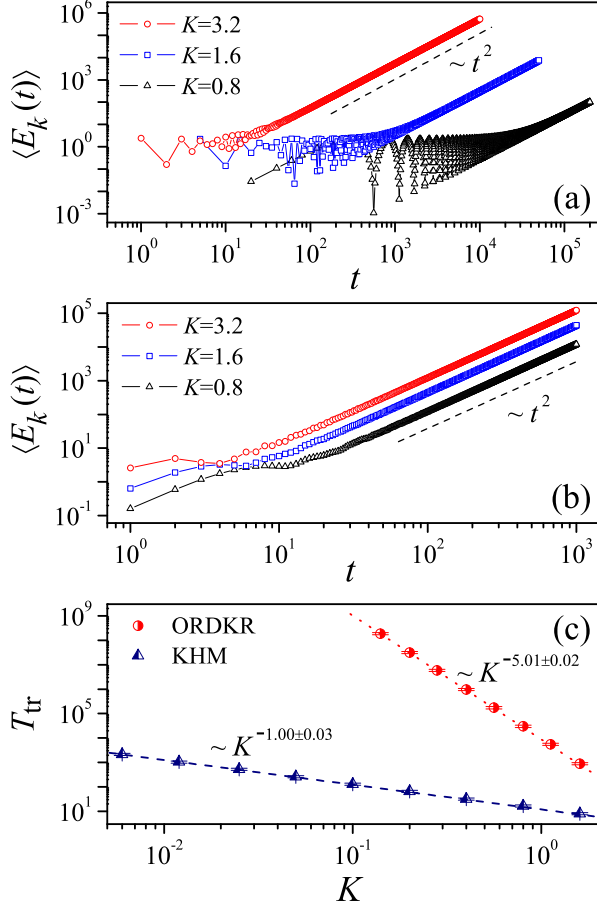


FIG. 4: (color online) Panels (a) and (b) depict the expectation value of system's kinetic energy versus time  $t$  (measured as the number of quantum maps iterated), with  $\hbar = 2\pi/3$  and the initial state given by  $|0\rangle$ , for three values of kick strength  $K = L$ , with (a) for ORDKR and (b) for KHM. For a small value of  $K$ , the kinetic energy of ORDKR or KHM is seen to be localized for a long while before it starts to increase ballistically. Panel (c) shows how the time scale of this initial transient stage, denoted  $T_{\text{tr}}$ , scales with  $K$ : the scaling is found to be  $\sim K^{-5}$  for ORDKR but  $\sim K^{-1}$  for KHM, which is consistent with our analysis of the respective bandwidth power-law scaling with  $K$ .

over a time scale before it starts to increase ballistically. The time scale of the freezing stage is shown to increase rapidly as we decrease the value of  $K$ . As a comparison, Figure 4(b) shows the parallel dynamics of KHM, for the same three values of  $K$ . There it is seen that the transient stage of localization is only weakly dependent upon  $K$ , which is again consistent with the linear  $K$ -dependence of the bandwidth of KHM. Quantitatively, the transient localization time scale  $T_{\text{tr}}$  is numerically determined from the duration of kinetic energy freezing. The  $T_{\text{tr}}$  thus obtained numerically and shown in Fig. 4(c) indeed satisfies the scaling  $T_{\text{tr}} \sim K^{-(N+2)}$  for ORDKR, which is in sharp contrast to the  $T_{\text{tr}} \sim K^{-1}$  scaling for KHM. The results here can also be understood as a quantitative explanation of our earlier finding of transient dynamical localization in Ref. [15]. For future experiments, the observation of the aforementioned scaling of  $T_{\text{tr}}$  versus  $K$  may serve as the first piece of evidence of a successful realization of an ORDKR.

### III. TOPOLOGICAL EQUIVALENCE BETWEEN ORDKR AND KHM

In this section, we devote ourselves to a detailed comparison of the Floquet band topologies of ORDKR and KHM. We first describe our motivation and introduce new notation. Next, we report numerical findings of the Floquet band topological numbers of both models. Finally, an exact analytical proof of the topological equivalence between ORDKR and KHM is presented.

#### A. Motivation and Notation

One early study [6] suggested that topological properties of the Floquet bands of KHM may be connected with the regular-to-chaos transition in the classical limit. Because ORDKR and KHM share the same classical limit (up to a canonical transformation), we suspect that there should be some similarity in their Floquet band topologies. Our second motivation for a topological study is related to an earlier finding that, when  $\hbar/(2\pi)$  is a *rational* number, the spectral union of  $U_{\text{ORDKR}-\alpha}$  (variant of ORDKR defined below) over all  $\alpha$  is the same as that of  $U_{\text{KHM}-\alpha}$  (variant KHM defined below) over all  $\alpha$  [17]. This previous mathematical result further suggests a possible topological connection between the two models. Interestingly, as we explore this possible topological connection, we are able to see a connec-

tion between KHM propagator and ORDKR propagator for each individual value of  $\alpha$  along with an individual value of the Bloch phase, thus going beyond Ref. [17] that considered a unification of all values of  $\alpha$  and the Bloch phase. Further, as we shall see below, the connection is established by a mapping in the parameter space, which cannot be achieved by a unitary transformation between the two propagators.

Next, we introduce necessary notation for our discussion of band topology. To characterize the band topology for both ORDKR and KHM, we introduce an additional periodic phase parameter  $\alpha \in [0, 2\pi)$  to the ORDKR and KHM maps, namely,

$$\begin{aligned} U_{\text{ORDKR}-\alpha} &= e^{i\frac{p^2}{2\hbar}} e^{-i\frac{K}{\hbar} \cos(q)} e^{-i\frac{p^2}{2\hbar}} e^{-i\frac{L}{\hbar} \cos(q+\alpha)} \\ U_{\text{KHM}-\alpha} &= e^{-i\frac{L}{\hbar} \cos(p-\alpha)} e^{-i\frac{K}{\hbar} \cos(q)}. \end{aligned} \quad (10)$$

For  $\hbar = 2\pi M/N$ , both operators are periodic in (angular) momentum space with period  $N\hbar$ . Hence, their eigenvalues are  $2\pi$ -periodic in the Bloch phase  $\varphi$  and also in  $\alpha$ , giving rise to  $N$  *extended* Floquet bands which disperse as a function of  $\varphi$  and  $\alpha$ . These 2-dimensional bands may be topologically characterized by Chern numbers, denoted  $C_n$  for the  $n$ th band. In what follows, we denote  $|\psi_n(\varphi, \alpha)\rangle$  as an (generalized) eigenstate of either  $U_{\text{ORDKR}-\alpha}$  or  $U_{\text{KHM}-\alpha}$ , in the  $n$ th band, with an eigenvalue  $\exp[i\epsilon_n(\varphi, \alpha)]$ . Such a generalized eigenstate lives on the entire (angular) momentum space. We then denote  $\tilde{U}(\varphi, \alpha)$  as the reduced  $N \times N$  Floquet matrix constructed from either  $U_{\text{ORDKR}-\alpha}$  or  $U_{\text{KHM}-\alpha}$  using the method described at the beginning of Section II. We next define the state  $|\bar{\psi}_n(\varphi, \alpha)\rangle$ , which is  $|\psi_n(\varphi, \alpha)\rangle$  projected onto  $N$  sites of one unit cell in the (angular) momentum space, i.e.,  $|\bar{\psi}_n(\varphi, \alpha)\rangle \equiv \sum_{m=0}^{N-1} |m\rangle \langle m|\psi_n(\varphi, \alpha)\rangle$ . We further assume that  $|\bar{\psi}_n(\varphi, \alpha)\rangle$  is normalized over one unit cell consisting of  $N$  sites. Using the above notation, the Berry curvature of the  $n$ th band is then defined as [24]

$$B_n(\varphi, \alpha) = i \sum_{n'=1, \neq n}^N \left\{ \frac{\langle \bar{\psi}_n | \frac{\partial \tilde{U}^\dagger}{\partial \varphi} | \bar{\psi}_{n'} \rangle \langle \bar{\psi}_{n'} | \frac{\partial \tilde{U}}{\partial \alpha} | \bar{\psi}_n \rangle}{|e^{-i\epsilon_n} - e^{-i\epsilon_{n'}}|^2} - \text{c.c.} \right\}, \quad (11)$$

where we have suppressed the explicit dependences on  $\varphi$  and  $\alpha$  for brevity. From the Berry curvature we obtain the Chern number  $C_n$ ,

$$C_n = \frac{1}{2\pi} \int_0^{2\pi} d\varphi \int_0^{2\pi} d\alpha B_n(\varphi, \alpha). \quad (12)$$

## B. Numerical Findings

We have conducted extensive numerical evaluations of the Floquet band Chern numbers associated with both  $U_{\text{ORDKR}-\alpha}$  and  $U_{\text{KHM}-\alpha}$ . We find that for the same  $K$  and  $L$  respectively in both models, the Chern numbers are always equal. For example, for  $\hbar = 2\pi/3$  and  $K = L$ , Fig. 5 represents the Floquet band Chern numbers for *both* models versus a varying  $K$ . The Chern numbers obtained for  $U_{\text{ORDKR}-\alpha}$  are identical with those for  $U_{\text{KHM}-\alpha}$ . Here, we adopt the convention that the band with largest absolute value of Chern number is always represented by the line in the middle. Vertical lines represent collisions between quasi-energy bands, during which Chern number transitions can take place. Note that in some cases band 1 and band 3 can collide directly with each other through the boundary of the quasienergy Brillouin zone. It is also important to stress that the Chern numbers of ORDKR match those of KHM for all  $K$  values, despite their jumps at various topological phase transition points. We are thus clearly witnessing, albeit numerically, a remarkable topological equivalence between ORDKR and KHM!

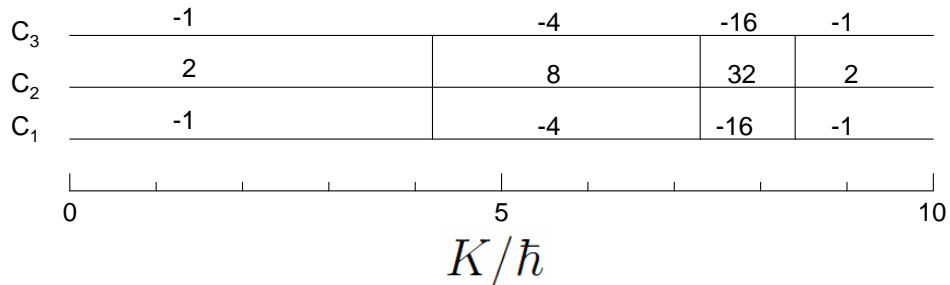


FIG. 5: Chern Numbers  $C_n$  for *both* ORDKR and KHM, for  $K = L$ . In both cases, topological phase transitions occur at  $K/\hbar \approx 4.20, 7.25, 8.40$  (correct to within  $\pm 0.05$ ).

Some insight into this observed topological equivalence may be obtained by comparing the quasienergy dispersions of the two models. In Fig. 6, we present the Floquet band structure for both ORDKR and KHM, in the case of  $K = L = 3\hbar$ . Interestingly, the ORDKR band profile appears to be the same as that of KHM, up to some translation along the  $\varphi$  and  $\alpha$  axes, followed by a rotation of the spectrum about the quasi-energy axis. This observation



is consistent with our proof of topological equivalence in the next section.

We have numerically observed that the topological equivalence also occurs for  $K \neq L$ . As one example of this, Fig. 7 depicts a zoo of Chern numbers for ORDKR and KHM, with  $\hbar = 2\pi/3$ ,  $L = \hbar$  fixed but  $K$  varying. We again see the same equivalence of Chern numbers across a few topological phase transition points. In addition, we found computationally that the Chern numbers are invariant upon an exchange between  $L$  and  $K$ . This was found to hold true also in other cases with more bands.

We have also plotted the Floquet band structure for a  $K > L$  case in Fig. 8. Here we consider the case of  $K/\hbar = 3$ ,  $L/\hbar = 1$ . It is seen that the band profiles of ORDKR and KHM are once again similar and appear to be related by a rotation and translation.

### C. Proof of Topological Equivalence

To strictly confirm our claim of topological equivalence, we present an analytical proof in this subsection. The proof proceeds as follows. We first show that the reduced ORDKR Floquet matrix and the reduced KHM Floquet matrix are equivalent up to a series of unitary transformations and a mapping between their parameter values. We then show that these matrices obtained under the unitary transformations and mapping of parameters still correspond to the same Chern numbers as the original reduced matrices. These steps constitute a proof of topological equivalence.

We consider cases with  $\hbar = 2\pi M/N$ , with  $M$  and  $N$  co-prime and both odd. In these cases, the reduced Floquet matrices of  $U_{\text{ORDKR}-\alpha}$  and  $U_{\text{KHM}-\alpha}$  (see the Appendix for details) can be written compactly as a product of  $N \times N$  unitary matrices

$$\begin{aligned}\tilde{U}_{\text{ORDKR}}(\varphi, \alpha) &= D_\varphi^\dagger D_1^\dagger (F^\dagger D_{1K} F) D_1 (F^\dagger D_{1L} F) D_\varphi \\ \tilde{U}_{\text{KHM}}(\varphi, \alpha) &= D_\varphi^\dagger D_{2L} (F^\dagger D_{2K} F) D_\varphi,\end{aligned}\tag{13}$$

where  $D_{1K}$ ,  $D_{1L}$ ,  $D_{2K}$ ,  $D_{2L}$  are diagonal unitary matrices, with matrix elements  $(D_{1K})_{n,m} = e^{i\frac{K}{\hbar} \cos(\frac{2\pi}{N}n - \frac{\varphi}{N})} \delta_{n,m}$ ,  $(D_{1L})_{n,m} = e^{-i\frac{L}{\hbar} \cos(\frac{2\pi}{N}n - \frac{\varphi}{N} + \alpha)} \delta_{n,m}$ ,  $(D_{2K})_{n,m} = e^{-i\frac{K}{\hbar} \cos(\frac{2\pi}{N}n - \frac{\varphi}{N})} \delta_{n,m}$ ,  $(D_{2L})_{n,m} = e^{-i\frac{L}{\hbar} \cos(n\hbar - \alpha)} \delta_{n,m}$ , where the index  $n$  takes values  $0, 1, \dots, N-1$ .  $D_1$  and  $D_\varphi$  are defined as they were in Section II.

We begin the proof by applying a unitary transformation given by  $U_1 \equiv F^\dagger D_{2K} F D_\varphi$  to the  $\tilde{U}_{\text{KHM}}(\varphi, \alpha)$  matrix to obtain  $\tilde{V}_{\text{KHM}}(\varphi, \alpha) \equiv U_1 \tilde{U}_{\text{KHM}}(\varphi, \alpha) U_1^\dagger$ . Writing  $F^\dagger D_{2K} F$  as the

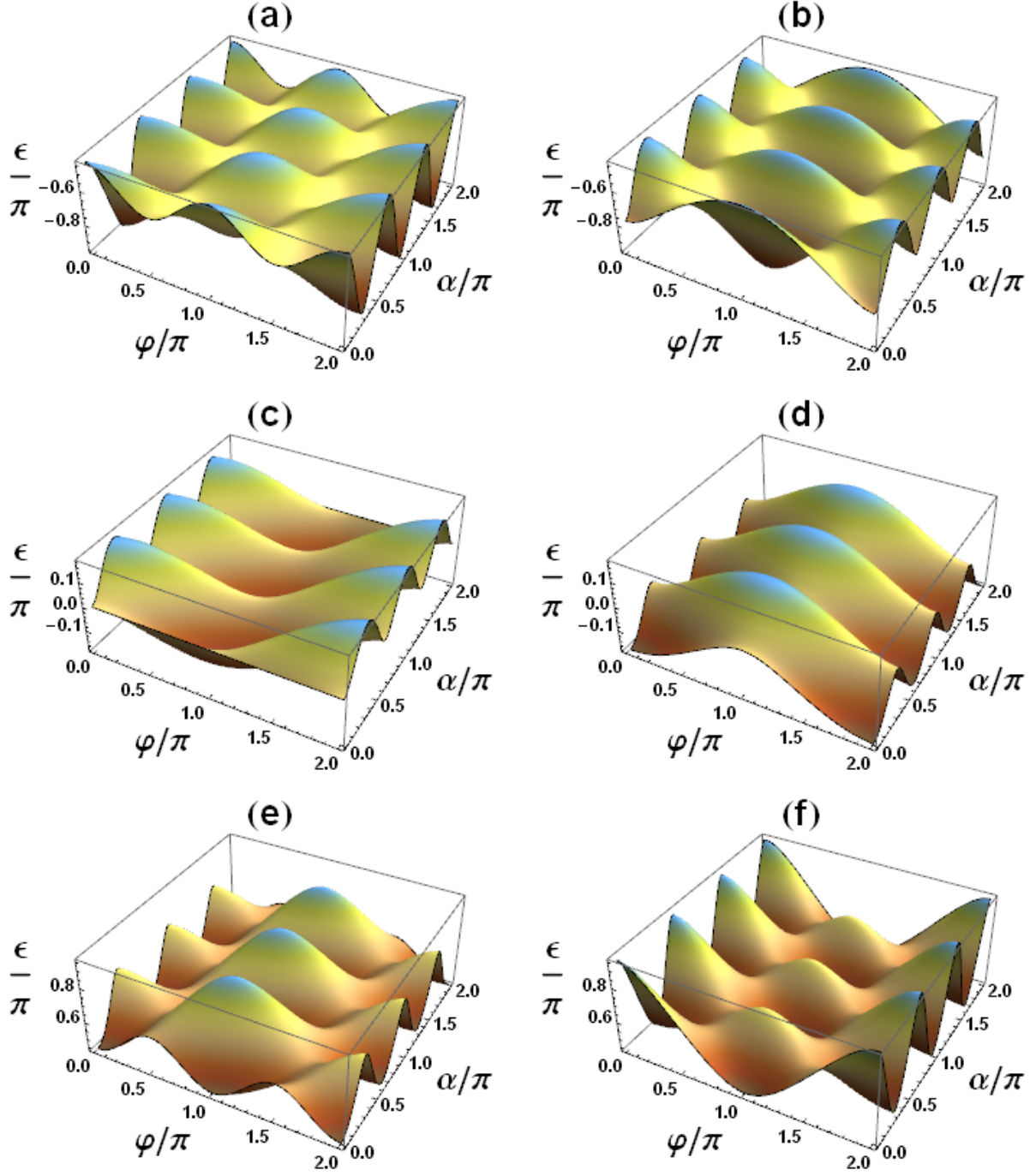


FIG. 6: (color online) Floquet band plots showing the quasienergy (eigenphase) dependence on  $\varphi$  and  $\alpha$  in ORDKR and KHM with  $K = L = 3\hbar$ ,  $\hbar = 2\pi/3$ . Figs. (a),(c),(e) [(b),(d),(f)] belong to bands 1,2 and 3 respectively for the ORDKR [KHM]. The ORDKR band profile appears to be a result of some translation along the  $\varphi$  and  $\alpha$  axes followed by a rotation of the spectrum about the  $\epsilon$  axis.

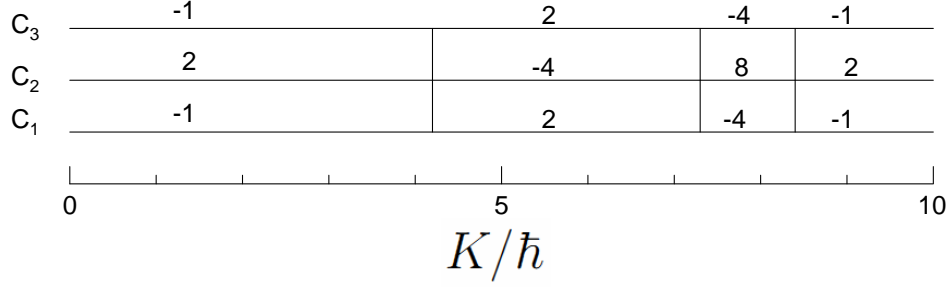


FIG. 7: Chern Numbers  $C_n$  for *both* ORDKR and KHM, with  $\hbar = 2\pi/3$ ,  $L = \hbar$  fixed, and a varying  $K$ . In both cases, topological phase transitions occur at  $K/\hbar \approx 4.20, 7.25, 8.40$  (correct to within  $\pm 0.05$ ). The Chern numbers obtained here are different from the case of  $K = L$  over some ranges of  $K$ . Note that the phase transition points seem to be exactly the same as those in Fig. 5 only because we have rounded the phase transition points to steps of 0.05. A more accurate characterization does show very small differences.

exponential of a matrix, we obtain

$$\begin{aligned}
\tilde{V}_{\text{KHM}}(\varphi, \alpha) &= F^\dagger D_{2K} F D_{2L} \\
&= \exp \left[ -i \frac{K}{2\hbar} F^\dagger \begin{pmatrix} \ddots & & & & \\ & e^{i(\frac{2\pi}{N}n - \frac{\varphi}{N})} + e^{-i(\frac{2\pi}{N}n - \frac{\varphi}{N})} & & & \\ & & \ddots & & \\ & & & \ddots & \\ & & & & \ddots \end{pmatrix} F \right] D_{2L} \\
&= \exp \left[ -i \frac{K}{2\hbar} \left( e^{-i\frac{\varphi}{N}} C + e^{i\frac{\varphi}{N}} C^\dagger \right) \right] \begin{pmatrix} \ddots & & & & \\ & e^{-i\frac{L}{\hbar} \cos(2\pi\frac{M}{N}n - \alpha)} & & & \\ & & \ddots & & \\ & & & \ddots & \\ & & & & \ddots \end{pmatrix},
\end{aligned} \tag{14}$$

where

$$C = \begin{pmatrix} 0 & 0 & \cdots & 0 & 1 \\ 1 & 0 & \cdots & 0 & 0 \\ 0 & 1 & \cdots & 0 & 0 \\ \vdots & \vdots & \ddots & \vdots & \vdots \\ 0 & 0 & \cdots & 1 & 0 \end{pmatrix}. \tag{15}$$

In the following steps, we will apply a series of unitary transformations to the reduced matrix  $\tilde{U}_{\text{ORDKR}}(\varphi, \alpha)$  and show that the result is equivalent to the above unitarily transformed

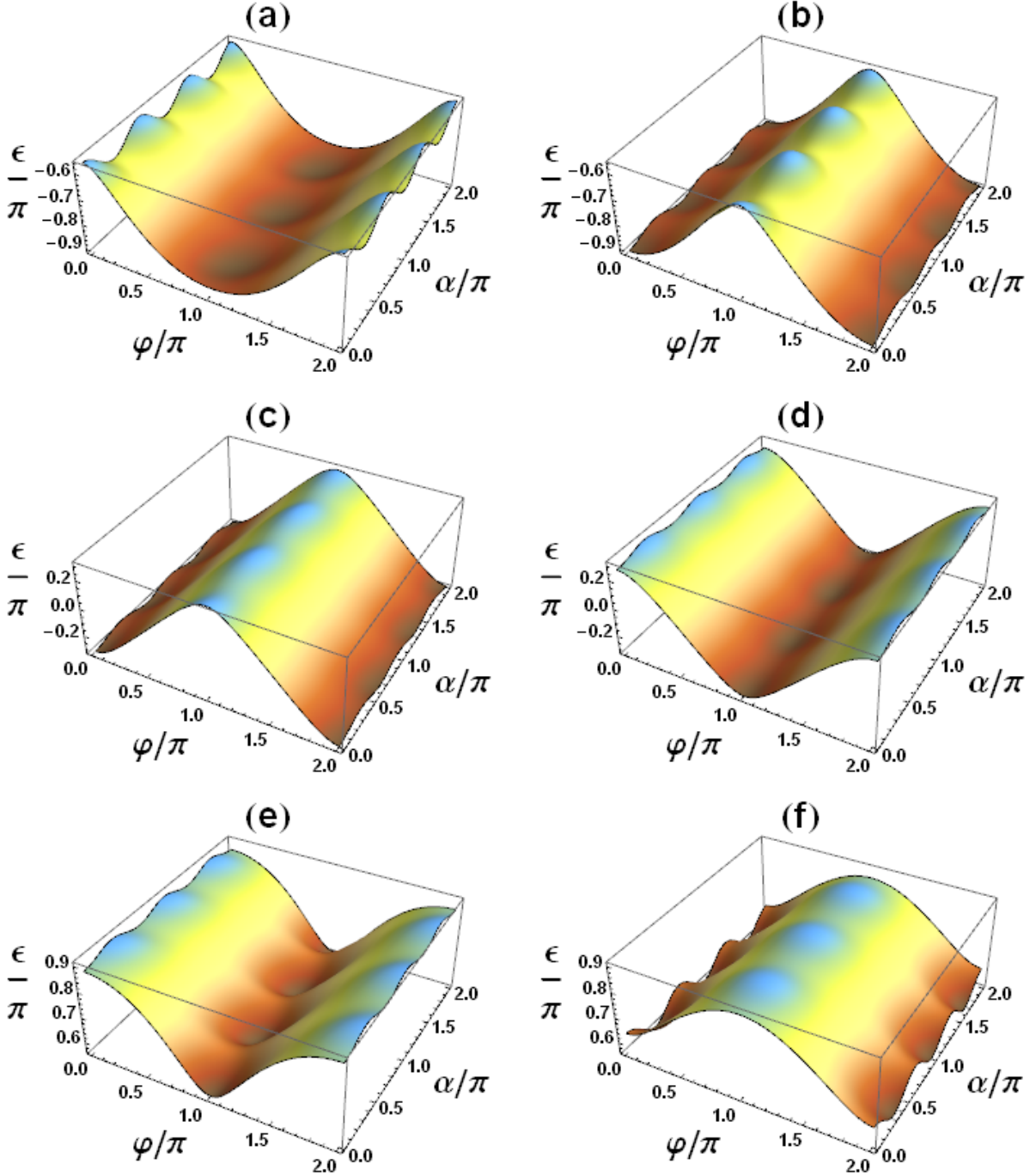


FIG. 8: (color online) Floquet band plots showing the quasienergy (eigenphase) dependence on  $\varphi$  and  $\alpha$ , for ORDKR and KHM with  $K = 3\hbar, L = \hbar$ ,  $\hbar = 2\pi/3$ . Figures (a),(c),(e) [(b),(d),(f)] belong to bands 1,2 and 3 respectively for the ORDKR [KHM].

version of  $\tilde{U}_{\text{KHM}}(\varphi, \alpha)$  provided a condition between  $\varphi$  and  $\alpha$  in the two models is obeyed.

Applying a transformation given by  $FD_\varphi$  to  $\tilde{U}_{\text{ORDKR}}(\varphi, \alpha)$ , we obtain  $\tilde{U}_{\text{ORDKR}}^{(1)}(\varphi, \alpha) \equiv$

$FD_\varphi \tilde{U}_{\text{ORDKR}}(\varphi, \alpha) D_\varphi^\dagger F^\dagger$ , which we simplify as follows.

$$\begin{aligned}
\tilde{U}_{\text{ORDKR}}^{(1)}(\varphi, \alpha) &= FD_1^\dagger F^\dagger D_{1K} F D_1 F^\dagger D_{1L} \\
&= FD_1^\dagger \exp \left[ i \frac{K}{2\hbar} \left( e^{-i\frac{\varphi}{N}} C + e^{i\frac{\varphi}{N}} C^\dagger \right) \right] D_1 F^\dagger D_{1L} \\
&= \exp \left[ i \frac{K}{2\hbar} \left( e^{-i\frac{\varphi}{N}} F D_1^\dagger C D_1 F^\dagger + e^{i\frac{\varphi}{N}} F D_1^\dagger C^\dagger D_1 F^\dagger \right) \right] D_{1L}.
\end{aligned} \tag{16}$$

Denoting  $X = FD_1^\dagger C D_1 F^\dagger$ ,  $\tilde{U}_{\text{ORDKR}}^{(1)}(\varphi, \alpha) = \exp \left[ i \frac{K}{2\hbar} \left( e^{-i\frac{\varphi}{N}} X + e^{i\frac{\varphi}{N}} X^\dagger \right) \right] D_{1L}$ . The explicit expression for  $X$  is

$$X = e^{i\pi \frac{N-M}{N}} \begin{pmatrix} & e^{i\frac{2\pi}{N} \times M} & \dots & 0 \\ & \vdots & \ddots & \vdots \\ & 0 & \dots & e^{i\frac{2\pi}{N} \times (N-1)} \\ e^{i\frac{2\pi}{N} \times 0} & \dots & 0 \\ \vdots & \ddots & \vdots \\ 0 & \dots & e^{i\frac{2\pi}{N} \times (M-1)} \end{pmatrix}. \tag{17}$$

Next, we introduce the  $N \times N$  permutation matrix  $P_\sigma$  which is made up entirely of zeroes except that in the  $j$ -th row, the  $\sigma_j$ -th column equals 1, with  $\sigma_j = j \times (N - M) \bmod N$ . Here,  $j$  and  $\sigma_j$  take values  $0, \dots, N - 1$ . Note that  $P_\sigma$  is unitary and that the set of  $\sigma_j$  values will include all of the  $N$  values  $j = 0, 1, \dots, N - 1$ . We apply the unitary transformation  $P_\sigma$  to  $\tilde{U}_{\text{ORDKR}}^{(1)}(\varphi, \alpha)$  and obtain  $\tilde{U}_{\text{ORDKR}}^{(2)}(\varphi, \alpha) \equiv P_\sigma \tilde{U}_{\text{ORDKR}}^{(1)}(\varphi, \alpha) P_\sigma^\dagger = \exp \left[ i \frac{K}{2\hbar} \left( e^{-i\frac{\varphi}{N}} P_\sigma X P_\sigma^\dagger + e^{i\frac{\varphi}{N}} P_\sigma X^\dagger P_\sigma^\dagger \right) \right] D'_{1L}$ , where  $D'_{1L} \equiv P_\sigma D_{1L} P_\sigma^\dagger$ .  $D'_{1L}$  is a diagonal unitary matrix with diagonal elements  $(D'_{1L})_{n,n} = e^{-i\frac{L}{\hbar} \cos(\frac{2\pi}{N} \sigma_n - \frac{\varphi}{N} + \alpha)} = e^{-i\frac{L}{\hbar} \cos(-2\pi \frac{M}{N} n - \frac{\varphi}{N} + \alpha)}$ .

The effect of the permutation matrix on  $X$  is as follows.

$$P_\sigma X P_\sigma^\dagger = e^{i\pi \frac{N-M}{N}} \begin{pmatrix} 0 & 0 & \dots & 0 & e^{i\frac{2\pi}{N} \sigma_{N-1}} \\ e^{i\frac{2\pi}{N} \sigma_0} & 0 & \dots & 0 & 0 \\ 0 & e^{i\frac{2\pi}{N} \sigma_1} & & 0 & 0 \\ \vdots & \vdots & \ddots & \vdots & \vdots \\ 0 & 0 & \dots & e^{i\frac{2\pi}{N} \sigma_{N-2}} & 0 \end{pmatrix} \tag{18}$$

We can see that the structure of the above matrix is very similar to  $C$  and would be made identical with it if we were to replace all the nonzero elements with 1. This is achieved by a transformation via the diagonal unitary matrix  $D_0$  which has diagonal elements  $(D_0)_{n,n} = e^{-i \left[ \frac{2\pi}{N} \sum_{k=0}^{k=n-1} \sigma_k + \pi \frac{N-M}{N} n \right]}$ . It can be shown that  $D_0 P_\sigma X P_\sigma^\dagger D_0^\dagger = C$ . Denoting  $\tilde{V}_{\text{ORDKR}}(\varphi, \alpha) \equiv$

$D_0 \tilde{U}_{\text{ORDKR}}^{(2)}(\varphi, \alpha) D_0^\dagger$  and using that  $D_0$  and  $D'_{1L}$  commute due to their both being diagonal, we obtain

$$\begin{aligned} \tilde{V}_{\text{ORDKR}}(\varphi, \alpha) &= \exp \left[ i \frac{K}{2\hbar} \left( e^{-i\frac{\varphi}{N}} C + e^{i\frac{\varphi}{N}} C^\dagger \right) \right] D'_{1L} \\ &= \exp \left[ -i \frac{K}{2\hbar} \left( e^{-i\frac{\varphi+N\pi}{N}} C + e^{i\frac{\varphi+N\pi}{N}} C^\dagger \right) \right] \begin{pmatrix} \ddots & & & \\ & e^{-i\frac{L}{\hbar} \cos(2\pi\frac{M}{N}j + \frac{\varphi}{N} - \alpha)} & & \\ & & \ddots & \\ & & & \ddots \end{pmatrix}. \end{aligned} \quad (19)$$

From Eq. (14) and (19), we observe that  $\tilde{V}_{\text{ORDKR}}(\varphi, \alpha)$  and  $\tilde{V}_{\text{KHM}}(\tilde{\varphi}, \tilde{\alpha})$  are identical, provided that  $\tilde{\varphi} = \varphi + N\pi$  and  $\tilde{\alpha} = \alpha - \frac{\varphi}{N}$ . Summarizing what we have found so far, we have learned that if we unitarily transform from  $\tilde{U}_{\text{KHM}}(\tilde{\varphi}, \tilde{\alpha})$  to  $\tilde{V}_{\text{KHM}}(\tilde{\varphi}, \tilde{\alpha}) \equiv U_1 \tilde{U}_{\text{KHM}}(\tilde{\varphi}, \tilde{\alpha}) U_1^\dagger$ , where  $U_1 \equiv F^\dagger D_{2K} F D_{\tilde{\varphi}}$ , and unitarily transform from  $\tilde{U}_{\text{ORDKR}}(\varphi, \alpha)$  to  $\tilde{V}_{\text{ORDKR}}(\varphi, \alpha) \equiv U_2 \tilde{U}_{\text{ORDKR}}(\varphi, \alpha) U_2^\dagger$ , where  $U_2 \equiv D_0 P_\sigma F D_\varphi$ , we find that the two unitarily transformed matrices are identical up to some mapping between  $(\tilde{\varphi}, \tilde{\alpha})$  and  $(\varphi, \alpha)$ .

Figure 9 represents one example of the quasi-energy band plot for both ORDKR and KHM. Referring to panel (b) and panel (c), we thus directly see that provided that  $\tilde{\varphi} = \varphi + N\pi$  and  $\tilde{\alpha} = \alpha - \frac{\varphi}{N}$ , the extended Floquet band structure for ORDKR and KHM are the same (though the boundaries on the  $(\tilde{\varphi}, \tilde{\alpha})$  plane are different).

Recapping our proof so far, with the mapping  $\tilde{\varphi} = \varphi + N\pi$  and  $\tilde{\alpha} = \alpha - \frac{\varphi}{N}$ , we have the following

$$\tilde{U}_{\text{KHM}}(\tilde{\varphi}, \tilde{\alpha}) = U_T \tilde{U}_{\text{ORDKR}}(\varphi, \alpha) U_T^\dagger, \quad (20)$$

where  $U_T \equiv D_{\tilde{\varphi}}^\dagger F^\dagger D_{2K}^\dagger(\tilde{\varphi}) F D_0 P_\sigma F D_\varphi$ , and the definitions of the matrices  $D$ ,  $F$ ,  $D_{2K}$ ,  $D_0$  and  $P_\sigma$  all are previously given. For example,  $(D_{\tilde{\varphi}})_{n,m} = e^{-in\frac{\tilde{\varphi}}{N}} \delta_{n,m}$ , and  $(D_{2K})(\tilde{\varphi})_{n,m} = e^{-i\frac{K}{\hbar} \cos(\frac{2\pi}{N}n - \frac{\tilde{\varphi}}{N})} \delta_{n,m}$ . Let  $|\bar{\psi}_n^{\text{KHM}}(\tilde{\varphi}, \tilde{\alpha})\rangle$  be the  $n$ th eigenstate of  $\tilde{U}_{\text{KHM}}(\tilde{\varphi}, \tilde{\alpha})$  and  $|\bar{\psi}_n^{\text{ORDKR}}(\varphi, \alpha)\rangle$  be the  $n$ th eigenstate of  $\tilde{U}_{\text{ORDKR}}(\varphi, \alpha)$ . Equation (20) then leads to

$$|\bar{\psi}_n^{\text{KHM}}(\tilde{\varphi}, \tilde{\alpha})\rangle = U_T |\bar{\psi}_n^{\text{ORDKR}}(\varphi, \alpha)\rangle. \quad (21)$$

Because scanning all the values of  $(\varphi, \alpha)$  will scan all the values of  $(\tilde{\varphi}, \tilde{\alpha})$ , it is obvious now that the union of the spectrum of  $\tilde{U}_{\text{KHM}}(\tilde{\varphi}, \tilde{\alpha})$  (after considering all values of  $\tilde{\varphi}$  and  $\tilde{\alpha}$ ) should be the same as the union of the spectrum of  $\tilde{U}_{\text{ORDKR}}(\varphi, \alpha)$  (after considering all values of  $\varphi$  and  $\alpha$ ), thus directly confirming an early proof in Ref. [17]. We stress, however, that the one-to-one correspondence between  $\tilde{U}_{\text{ORDKR}}(\varphi, \alpha)$  and  $\tilde{U}_{\text{KHM}}(\varphi, \alpha)$  is a new result that we did not find previously.

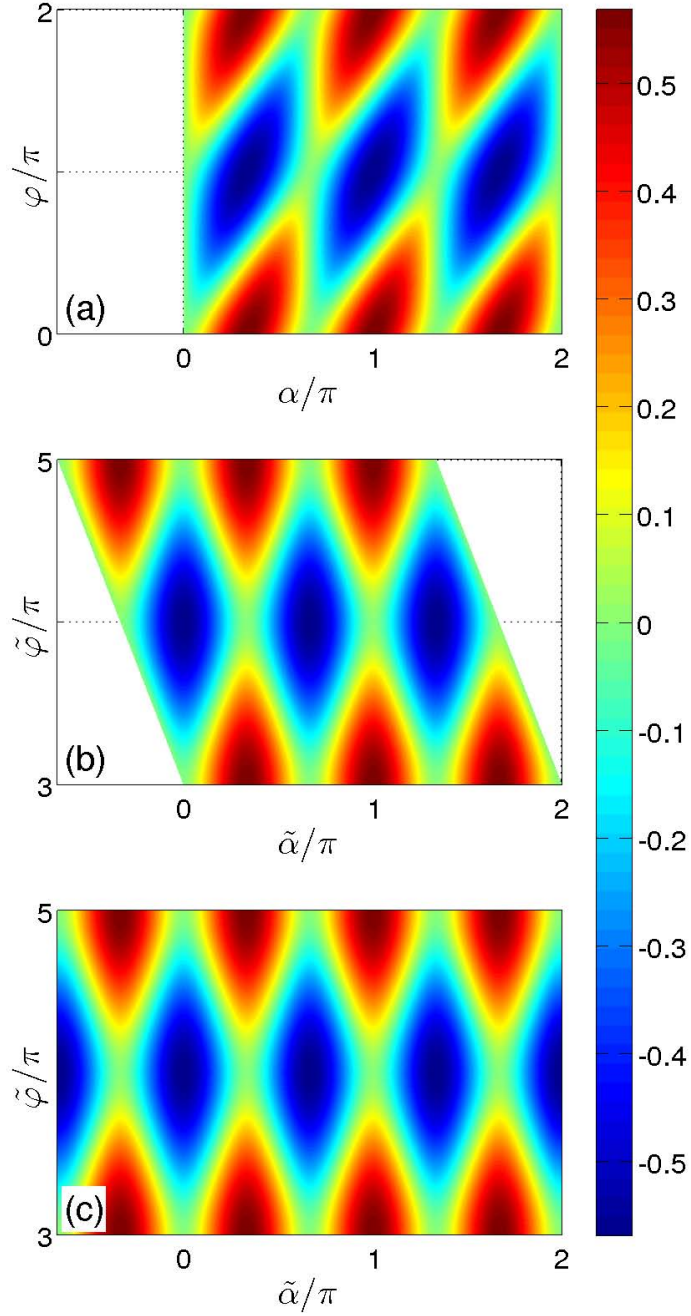


FIG. 9: (color online) Quasi-energy band (band 2) plot for  $K = L = 3\hbar$  with  $\hbar = 2\pi/3$ . Panel (a) shows dependence on  $(\varphi, \alpha)$  for  $\tilde{U}_{\text{ORDKR}}(\varphi, \alpha)$ , whereas panel (b) shows dependence on  $(\tilde{\varphi}, \tilde{\alpha})$  for  $\tilde{U}_{\text{ORDKR}}(\tilde{\varphi} - N\pi, \tilde{\alpha} + \frac{\tilde{\varphi}}{N} - \pi)$ . Panel (c) shows dependence on  $(\tilde{\varphi}, \tilde{\alpha})$  for  $\tilde{U}_{\text{KHM}}(\tilde{\varphi}, \tilde{\alpha})$ .

Finally, we show that  $\tilde{V}_{\text{ORDKR}}(\varphi, \alpha)$  and  $\tilde{V}_{\text{KHM}}(\varphi, \alpha)$  have the same set of Chern numbers as their respective original matrices  $\tilde{U}_{\text{ORDKR}}(\varphi, \alpha)$  and  $\tilde{U}_{\text{KHM}}(\varphi, \alpha)$ . To do this, we make use

of the line integral version of the Chern number of the  $n$ th band given by

$$C_n = \frac{i}{2\pi} \oint d\vec{\theta} \langle \bar{\psi}_n(\vec{\theta}) | \partial_{\vec{\theta}} | \bar{\psi}_n(\vec{\theta}) \rangle, \quad (22)$$

where  $\vec{\theta} \equiv (\varphi, \alpha)$  and the line integral is around the perimeter of the Brillouin zone  $(0, 2\pi] \times (0, 2\pi]$  in  $(\varphi, \alpha)$  parameter space. Here  $| \bar{\psi}_n(\vec{\theta}) \rangle$  again refers to the  $n$ th band eigenstate of either  $\tilde{U}_{\text{ORDKR}}(\varphi, \alpha)$  or  $\tilde{U}_{\text{KHM}}(\varphi, \alpha)$  at the point  $\vec{\theta}$ . The eigenstates of  $\tilde{V}_{\text{KHM}}(\varphi, \alpha)$  and  $\tilde{V}_{\text{ORDKR}}(\varphi, \alpha)$ , denoted  $| \tilde{\psi}_n(\vec{\theta}) \rangle$ , are related to the original eigenstates by  $U_{1,2}^\dagger | \tilde{\psi}_n(\vec{\theta}) \rangle = | \bar{\psi}_n(\vec{\theta}) \rangle$  respectively. We may substitute this into Eq. (22) and obtain an expression for  $C_n$  in terms of  $| \tilde{\psi}_n(\vec{\theta}) \rangle$ . Because the transformations  $U_{1,2}$  depend on  $\varphi$  but not on  $\alpha$ , it can be shown, by making use of the fact that the line integrals along  $\alpha = 0$  and  $\alpha = 2\pi$  are in opposite directions, that the resulting expression for  $C_n$  reduces back to that of the form of Eq. (22), except with the transformed eigenstates taking the place of the original ones. This proves that the Chern numbers of the unitarily transformed reduced matrices match those of the original ones.

Next, we note that when we impose  $\tilde{\varphi} = \varphi + N\pi$  and  $\tilde{\alpha} = \alpha - \frac{\varphi}{N}$ , working out the line integral in Eq. (22) for  $\tilde{V}_{\text{ORDKR}}(\varphi, \alpha)$  over a typical square perimeter space in  $(\varphi, \alpha)$  space with corners  $(0, 0), (2\pi, 0), (2\pi, 2\pi), (0, 2\pi)$  is equivalent to working out the line integral for  $\tilde{V}_{\text{KHM}}(\tilde{\varphi}, \tilde{\alpha})$  over some parallelogram in  $(\tilde{\varphi}, \tilde{\alpha})$  space with corners  $(N\pi, 0), (N\pi + 2\pi, -2\pi/N), (N\pi + 2\pi, 2\pi - 2\pi/N), (N\pi, 2\pi)$ . To complete the proof of topological equivalence, we need only show that the aforementioned line integral in  $(\tilde{\varphi}, \tilde{\alpha})$  for  $\tilde{V}_{\text{KHM}}(\tilde{\varphi}, \tilde{\alpha})$  gives a result equal to that when we calculate the line integral around the perimeter of the usual  $(0, 2\pi] \times (0, 2\pi]$  Brillouin zone. However, this can be easily shown to be the case by converting the line integral around the parallelogram into a surface integral using Stokes' theorem. We then obtain a surface integral of the form of Eq. (12) enclosing the area of the parallelogram. Because the Berry curvature as seen in Eq. (11) is exactly  $2\pi$ -periodic along both  $\varphi$  and  $\alpha$ , it is trivial to see that we can map the area of the parallelogram back onto that of the original  $(0, 2\pi] \times (0, 2\pi]$  Brillouin zone, without any difference in the result of the integral. In other words, the Chern numbers of  $\tilde{V}_{\text{KHM}}(\tilde{\varphi}, \tilde{\alpha})$  and  $\tilde{V}_{\text{ORDKR}}(\varphi, \alpha)$  are always identical. Putting this together with the result of the previous paragraph, we may conclude that the Chern numbers of the original matrices  $\tilde{U}_{\text{KHM}}(\varphi, \alpha)$  and  $\tilde{U}_{\text{ORDKR}}(\varphi, \alpha)$  are indeed the same. This completes our proof of topological equivalence.



#### IV. CONCLUDING REMARKS

In this work, we have mainly focused on two topics: the spectral difference between ORDKR and KHM (comparing quantum maps  $U_{\text{ORDKR}}$  and  $U_{\text{KHM}}$ ) and their topological equivalence upon introducing an additional periodic phase parameter  $\alpha$  (comparing quantum maps  $U_{\text{ORDKR}-\alpha}$  and  $U_{\text{KHM}-\alpha}$ ). One important spectral difference we have found is the existence of a flat band for  $U_{\text{ORDKR}}$  under the condition  $K = L$ , but not for  $U_{\text{KHM}}$ . To our knowledge, this is the first example of a periodically driven model that has a mixture of flat band and non-flat bands. States launched from a flat band will be strictly localized, and this feature might be useful for benchmarking experimental errors in any future realizations of ORDKR. The coexistence of a flat band with non-flat bands may also open up new applications of  $\delta$ -kicked systems. We have also shown that for small kick strength  $K = L$ , the band width of the non-flat bands of  $U_{\text{ORDKR}}$  scales with  $K$  in a power law with a high exponent  $N + 2$ , indicating that for sufficiently small kick strength, all Floquet bands will be effectively flat for a long time scale. The dynamical consequence is a transient dynamical localization in ORDKR (absent in KHM) for a long time scale. The topological equivalence between  $U_{\text{ORDKR}-\alpha}$  and  $U_{\text{KHM}-\alpha}$  makes our ORDKR-KHM comparison even more interesting. That is, for a fixed  $\alpha$ , ORDKR and KHM have many different features. But topologically speaking, upon introducing one extra parameter  $\alpha$  we have a topological equivalence between an extended ORDKR model, previously proposed in studies of quantum ratchet acceleration without using a bichromatic lattice [27], with a simple extension of the standard KHM. To have a pair of models that are topologically equivalent should be a useful contribution to the general understanding of the topological properties of periodically driven systems [28].

#### V. ACKNOWLEDGMENTS

J.W. and J.G. acknowledge helpful discussions with Prof. Italo Guarneri, who also confirmed our flat-band result by showing us an alternative proof by him. D.H. thanks Adam Zaman Chaudhry for helpful discussions. J.W. received support from NNSF (Grants No.11275159 and No. 10925525) and SRFDP (Grant No. 20100121110021) of China, and J.G. is supported by ARF Tier I, MOE of Singapore (Grant No. R-144-000-276-112). J.G.

dedicates this work to his late beloved wife Huairui Zhang.

## Appendix A: Expressions for reduced Floquet matrices

For  $\hbar = 2\pi M/N$  with  $M$  and  $N$  being coprime and odd integers, reduced  $N \times N$  Floquet matrix is given by  $\left[ \tilde{U}(\varphi) \right]_{n,m} = \sum_{l=-\infty}^{\infty} \langle n | \hat{U} | m + l \times N \rangle e^{il\varphi}$ .

### 1. Reduced Floquet matrix for ORDKR

The Floquet operator of ORDKR is

$$U_{\text{ORDKR}} = e^{i\frac{p^2}{2\hbar}} e^{-i\frac{K}{\hbar} \cos(q)} e^{-i\frac{p^2}{2\hbar}} e^{-i\frac{L}{\hbar} \cos(q)}. \quad (\text{A1})$$

The reduced  $N \times N$  Floquet matrix is thus

$$\begin{aligned} \left[ \tilde{U}_{\text{ORDKR}}(\varphi) \right]_{n,m} &= \sum_{l=-\infty}^{\infty} \langle n | \hat{U}_{\text{ORDKR}} | m + l \times N \rangle e^{il\varphi} \\ &= \sum_{l=-\infty}^{\infty} \sum_{l'=-\infty}^{\infty} \sum_{m'=0}^{N-1} \langle n | e^{i\frac{p^2}{2\hbar}} e^{-i\frac{K}{\hbar} \cos(q)} | m' + l' \times N \rangle \\ &\quad \times \langle m' + l' \times N | e^{-i\frac{p^2}{2\hbar}} e^{-i\frac{L}{\hbar} \cos(q)} | m + l \times N \rangle e^{il\varphi} \\ &= \sum_{m'=0}^{N-1} \frac{1}{2\pi} e^{i\frac{\hbar}{2}n^2} \int_0^{2\pi} d\theta_2 e^{-i\frac{K}{\hbar} \cos(\theta_2)} e^{i\theta_2(m'-n)} \sum_{l'=-\infty}^{\infty} e^{i\theta_2 l' N} \\ &\quad \times \frac{1}{2\pi} e^{-i\frac{\hbar}{2}(m'+l'N)^2} \int_0^{2\pi} d\theta_1 e^{-i\frac{L}{\hbar} \cos(\theta_1)} e^{i\theta_1(m-m')} \sum_{l=-\infty}^{\infty} e^{i\theta_1(l-l')N} e^{il\varphi} \\ &= \sum_{m'=0}^{N-1} \frac{1}{2\pi} e^{i\frac{\hbar}{2}n^2} \int_0^{2\pi} d\theta_2 e^{i\frac{K}{\hbar} \cos(\theta_2+\pi)} e^{i(\theta_2+\pi)(m'-n)} e^{i\pi(m'-n)} \sum_{l'=-\infty}^{\infty} e^{i(\theta_2+\pi)l'N} \\ &\quad \times \frac{1}{2\pi} e^{-i\frac{\hbar}{2}m'^2} \int_0^{2\pi} d\theta_1 e^{-i\frac{L}{\hbar} \cos(\theta_1)} e^{i\theta_1(m-m')} e^{-i\theta_1 l' N} \sum_{l=-\infty}^{\infty} e^{i\theta_1 l N} e^{il\varphi}. \end{aligned} \quad (\text{A2})$$

To simplify, we make use of the Poisson summation formula

$$\sum_{l=-\infty}^{\infty} e^{2\pi il\varphi} = \sum_{j=-\infty}^{\infty} \delta(\varphi - j), \quad (\text{A3})$$

and obtain

$$\begin{aligned}
\left[ \tilde{U}_{\text{ORDKR}}(\varphi) \right]_{n,m} &= e^{i\frac{\hbar}{2}n^2} \sum_{m'=0}^{N-1} e^{-i\frac{\hbar}{2}m'^2} e^{i\pi(m'-n)} \frac{1}{N} \sum_{j_2=0}^{N-1} e^{i\frac{K}{\hbar} \cos(\frac{2\pi}{N}j_2 - \frac{\varphi}{N})} e^{i(\frac{2\pi}{N}j_2 - \frac{\varphi}{N})(m'-n)} \\
&\quad \times \frac{1}{N} \sum_{j_1=0}^{N-1} e^{-i\frac{L}{\hbar} \cos(\frac{2\pi}{N}j_1 - \frac{\varphi}{N})} e^{i(\frac{2\pi}{N}j_1 - \frac{\varphi}{N})(m-m')} \\
&= \frac{1}{N^2} \sum_{j_2=0}^{N-1} \sum_{m'=0}^{N-1} \sum_{j_1=0}^{N-1} e^{in\frac{\varphi}{N}} e^{-im\frac{\varphi}{N}} \\
&\quad \times e^{-i\frac{2\pi-\hbar}{2}n^2} e^{-i\frac{2\pi}{N}nj_2} e^{i\frac{K}{\hbar} \cos(\frac{2\pi}{N}j_2 - \frac{\varphi}{N})} e^{i\frac{2\pi}{N}j_2m'} \\
&\quad \times e^{i\frac{2\pi-\hbar}{2}m'^2} e^{-i\frac{2\pi}{N}m'j_1} e^{-i\frac{L}{\hbar} \cos(\frac{2\pi}{N}j_1 - \frac{\varphi}{N})} e^{i\frac{2\pi}{N}j_1m}.
\end{aligned} \tag{A4}$$

For the sake of illustration, we write the reduced Floquet matrix as a product of unitary matrices

$$\begin{aligned}
\tilde{U}_{\text{ORDKR}}(\varphi) &= \begin{pmatrix} \ddots & & \\ & e^{in\frac{\varphi}{N}} & \\ & & \ddots \end{pmatrix} \\
&\begin{pmatrix} \ddots & & \\ & e^{-i\frac{2\pi-\hbar}{2}n^2} & \\ & & \ddots \end{pmatrix} \begin{pmatrix} & & \\ & \frac{e^{-i\frac{2\pi}{N}nj_2}}{\sqrt{N}} & \\ & & \ddots \end{pmatrix} \begin{pmatrix} \ddots & & \\ & e^{i\frac{K}{\hbar} \cos(\frac{2\pi}{N}j_2 - \frac{\varphi}{N})} & \\ & & \ddots \end{pmatrix} \begin{pmatrix} & & \\ & \frac{e^{i\frac{2\pi}{N}j_2m'}}{\sqrt{N}} & \\ & & \ddots \end{pmatrix} \\
&\begin{pmatrix} \ddots & & \\ & e^{i\frac{2\pi-\hbar}{2}m'^2} & \\ & & \ddots \end{pmatrix} \begin{pmatrix} & & \\ & \frac{e^{-i\frac{2\pi}{N}m'j_1}}{\sqrt{N}} & \\ & & \ddots \end{pmatrix} \begin{pmatrix} \ddots & & \\ & e^{-i\frac{L}{\hbar} \cos(\frac{2\pi}{N}j_1 - \frac{\varphi}{N})} & \\ & & \ddots \end{pmatrix} \begin{pmatrix} & & \\ & \frac{e^{i\frac{2\pi}{N}j_1m}}{\sqrt{N}} & \\ & & \ddots \end{pmatrix} \\
&\begin{pmatrix} \ddots & & \\ & e^{-im\frac{\varphi}{N}} & \\ & & \ddots \end{pmatrix}
\end{aligned} \tag{A5}$$

If we introduce an additional periodic phase parameter  $\alpha \in [0, 2\pi)$  to the ORDKR map, the Floquet operator becomes

$$U_{\text{ORDKR}-\alpha} = e^{i\frac{p^2}{2\hbar}} e^{-i\frac{K}{\hbar} \cos(q)} e^{-i\frac{p^2}{2\hbar}} e^{-i\frac{L}{\hbar} \cos(q+\alpha)}. \tag{A6}$$

The corresponding reduced Floquet matrix is

$$\begin{aligned}
\left[ \tilde{U}_{\text{ORDKR}}(\varphi, \alpha) \right]_{n,m} &= \frac{1}{N^2} \sum_{j_2=0}^{N-1} \sum_{m'=0}^{N-1} \sum_{j_1=0}^{N-1} e^{in\frac{\varphi}{N}} e^{-im\frac{\varphi}{N}} \\
&\times e^{-i\frac{2\pi-\hbar}{2}n^2} e^{-i\frac{2\pi}{N}nj_2} e^{i\frac{K}{\hbar} \cos(\frac{2\pi}{N}j_2 - \frac{\varphi}{N})} e^{i\frac{2\pi}{N}j_2m'} \\
&\times e^{i\frac{2\pi-\hbar}{2}m'^2} e^{-i\frac{2\pi}{N}m'j_1} e^{-i\frac{L}{\hbar} \cos(\frac{2\pi}{N}j_1 - \frac{\varphi}{N} + \alpha)} e^{i\frac{2\pi}{N}j_1m}.
\end{aligned} \tag{A7}$$

Written again as a product of unitary matrices,

$$\begin{aligned}
\tilde{U}_{\text{ORDKR}}(\varphi, \alpha) &= \begin{pmatrix} \ddots & & & \\ & e^{in\frac{\varphi}{N}} & & \\ & & \ddots & \\ & & & \ddots \end{pmatrix} \\
&\begin{pmatrix} \ddots & & & \\ & e^{-i\frac{2\pi-\hbar}{2}n^2} & & \\ & & \ddots & \\ & & & \ddots \end{pmatrix} \begin{pmatrix} & & & \\ & \frac{e^{-i\frac{2\pi}{N}nj_2}}{\sqrt{N}} & & \\ & & \ddots & \\ & & & \ddots \end{pmatrix} \begin{pmatrix} \ddots & & & \\ & e^{i\frac{K}{\hbar} \cos(\frac{2\pi}{N}j_2 - \frac{\varphi}{N})} & & \\ & & \ddots & \\ & & & \ddots \end{pmatrix} \begin{pmatrix} & & & \\ & \frac{e^{i\frac{2\pi}{N}j_2m'}}{\sqrt{N}} & & \\ & & \ddots & \\ & & & \ddots \end{pmatrix} \\
&\begin{pmatrix} \ddots & & & \\ & e^{i\frac{2\pi-\hbar}{2}m'^2} & & \\ & & \ddots & \\ & & & \ddots \end{pmatrix} \begin{pmatrix} & & & \\ & \frac{e^{-i\frac{2\pi}{N}m'j_1}}{\sqrt{N}} & & \\ & & \ddots & \\ & & & \ddots \end{pmatrix} \begin{pmatrix} \ddots & & & \\ & e^{-i\frac{L}{\hbar} \cos(\frac{2\pi}{N}j_1 - \frac{\varphi}{N} + \alpha)} & & \\ & & \ddots & \\ & & & \ddots \end{pmatrix} \begin{pmatrix} & & & \\ & \frac{e^{i\frac{2\pi}{N}j_1m}}{\sqrt{N}} & & \\ & & \ddots & \\ & & & \ddots \end{pmatrix} \\
&\begin{pmatrix} \ddots & & & \\ & e^{-im\frac{\varphi}{N}} & & \\ & & \ddots & \\ & & & \ddots \end{pmatrix}
\end{aligned} \tag{A8}$$

## 2. Reduced Floquet matrix for KHM

The Floquet operator of KHM is

$$U_{\text{KHM}} = e^{-i\frac{L}{\hbar} \cos(p)} e^{-i\frac{K}{\hbar} \cos(q)}, \tag{A9}$$

with reduced  $N \times N$  Floquet matrix

$$\begin{aligned}
\left[ \tilde{U}_{\text{KHM}}(\varphi) \right]_{n,m} &= \sum_{l=-\infty}^{\infty} \langle n | \hat{U}_{\text{KHM}} | m + l \times N \rangle e^{il\varphi} \\
&= \frac{1}{2\pi} e^{-i\frac{L}{\hbar} \cos(nh)} \int_0^{2\pi} d\theta e^{-i\frac{K}{\hbar} \cos(\theta)} e^{i\theta(m-n)} \sum_{l=-\infty}^{\infty} e^{i\theta l N} e^{il\varphi} \\
&= e^{-i\frac{L}{\hbar} \cos(nh)} \frac{1}{N} \sum_{j=0}^{N-1} e^{-i\frac{K}{\hbar} \cos(\frac{2\pi}{N}j - \frac{\varphi}{N})} e^{i(\frac{2\pi}{N}j - \frac{\varphi}{N})(m-n)} \\
&= \frac{1}{N} \sum_{j=0}^{N-1} e^{in\frac{\varphi}{N}} e^{-i\frac{L}{\hbar} \cos(nh)} e^{-i\frac{2\pi}{N}nj} e^{i\frac{K}{\hbar} \cos(\frac{2\pi}{N}j - \frac{\varphi}{N})} e^{i\frac{2\pi}{N}jm} e^{-im\frac{\varphi}{N}}.
\end{aligned} \tag{A10}$$

For the sake of illustration, we write the reduced Floquet matrix as a product of unitary matrices.

$$\begin{aligned}
\tilde{U}_{\text{KHM}}(\varphi) &= \begin{pmatrix} \ddots & & & \\ & e^{in\frac{\varphi}{N}} & & \\ & & \ddots & \\ & & & \ddots \end{pmatrix} \\
&\begin{pmatrix} \ddots & & & \\ & e^{-i\frac{L}{\hbar} \cos(nh)} & & \\ & & \ddots & \\ & & & \ddots \end{pmatrix} \begin{pmatrix} e^{-i\frac{2\pi}{N}nj} \\ \sqrt{N} \end{pmatrix} \begin{pmatrix} \ddots & & & \\ & e^{-i\frac{K}{\hbar} \cos(\frac{2\pi}{N}j - \frac{\varphi}{N})} & & \\ & & \ddots & \\ & & & \ddots \end{pmatrix} \begin{pmatrix} e^{i\frac{2\pi}{N}jm} \\ \sqrt{N} \end{pmatrix} \\
&\begin{pmatrix} \ddots & & & \\ & e^{-im\frac{\varphi}{N}} & & \\ & & \ddots & \\ & & & \ddots \end{pmatrix}
\end{aligned} \tag{A11}$$

If we introduce an additional periodic phase parameter  $\alpha \in [0, 2\pi)$  to the KHM map, the Floquet operator becomes

$$U_{\text{KHM}-\alpha} = e^{-i\frac{L}{\hbar} \cos(p-\alpha)} e^{-i\frac{K}{\hbar} \cos(q)}. \tag{A12}$$

The corresponding reduced Floquet matrix is

$$\left[ \tilde{U}_{\text{KHM}}(\varphi, \alpha) \right]_{n,m} = \frac{1}{N} \sum_{j=0}^{N-1} e^{in\frac{\varphi}{N}} e^{-i\frac{L}{\hbar} \cos(nh-\alpha)} e^{-i\frac{2\pi}{N}nj} e^{i\frac{K}{\hbar} \cos(\frac{2\pi}{N}j - \frac{\varphi}{N})} e^{i\frac{2\pi}{N}jm} e^{-im\frac{\varphi}{N}}. \tag{A13}$$

Written as a product of unitary matrices,

$$\begin{aligned}
\tilde{U}_{\text{KHM}}(\varphi, \alpha) &= \begin{pmatrix} \ddots & & & \\ & e^{in\frac{\varphi}{N}} & & \\ & & \ddots & \\ & & & \ddots \end{pmatrix} \\
&\begin{pmatrix} \ddots & & & \\ & e^{-i\frac{L}{\hbar} \cos(n\hbar - \alpha)} & & \\ & & \ddots & \\ & & & \ddots \end{pmatrix} \begin{pmatrix} \frac{e^{-i\frac{2\pi}{N}nj}}{\sqrt{N}} \\ & & & \\ & & & \\ & & & \end{pmatrix} \begin{pmatrix} \ddots & & & \\ & e^{-i\frac{K}{\hbar} \cos(\frac{2\pi}{N}j - \frac{\varphi}{N})} & & \\ & & \ddots & \\ & & & \ddots \end{pmatrix} \begin{pmatrix} \frac{e^{i\frac{2\pi}{N}jm}}{\sqrt{N}} \\ & & & \\ & & & \\ & & & \end{pmatrix} \\
&\begin{pmatrix} \ddots & & & \\ & e^{-im\frac{\varphi}{N}} & & \\ & & \ddots & \\ & & & \ddots \end{pmatrix} \quad (A14)
\end{aligned}$$

### Appendix B: Calculation of symmetric $B$ matrix

$D_1$  is a diagonal unitary matrix and  $F$  is a unitary matrix. The corresponding matrix elements are  $[D_1]_{n,n} = e^{i\frac{2\pi - \hbar}{2}n^2}$ ,  $F_{m,n} = \frac{1}{\sqrt{N}}e^{i\frac{2\pi}{N}mn}$ , where  $\hbar = 2\pi\frac{M}{N}$ , and indices  $m$  and  $n$  take values  $0, 1, \dots, N-1$ . We also assume  $k$  is an integer ranging from 1 to  $N$ , and  $\tilde{k}$  is an integer ranging from 1 to  $Q$ , with  $Q = (N-1)/2$ . From  $B \equiv FD_1F^\dagger$  and using the fact

that  $MN$  is an odd number, we have

$$\begin{aligned}
B_{m,n} &= \frac{1}{N} \sum_{k=1}^N e^{i\frac{2\pi}{N} [\frac{M}{2}k^2 + (\frac{N}{2} + m - n)k]} \\
&= \frac{1}{N} \sum_{k=1}^N (-1)^k e^{i\frac{2\pi}{N} [\frac{M}{2}k^2 + (m-n)k]} \\
&= \frac{1}{N} \sum_{\tilde{k}=1}^Q e^{i\frac{2\pi}{N} [\frac{M}{2}(2\tilde{k})^2 + (m-n)(2\tilde{k})]} \\
&\quad - \frac{1}{N} \sum_{\tilde{k}=1}^Q e^{i\frac{2\pi}{N} [\frac{M}{2}(N-2\tilde{k})^2 + (m-n)(N-2\tilde{k})]} \\
&\quad - \frac{1}{N} e^{i\frac{2\pi}{N} [\frac{M}{2}N^2 + (m-n)N]} \\
&= \frac{1}{N} + \frac{1}{N} \sum_{\tilde{k}=1}^Q e^{i\frac{2\pi}{N} [2M\tilde{k}^2 + 2(m-n)\tilde{k}]} \\
&\quad - \frac{1}{N} \sum_{\tilde{k}=1}^Q e^{i\frac{2\pi}{N} [2M\tilde{k}^2 + \frac{M}{2}N^2 - 2MN\tilde{k} + (m-n)N - 2(m-n)\tilde{k}]} \\
&= \frac{1}{N} + \frac{1}{N} \sum_{\tilde{k}=1}^Q \left[ e^{i\frac{2\pi}{N} (2M\tilde{k}^2 + 2(m-n)\tilde{k})} + e^{i\frac{2\pi}{N} (2M\tilde{k}^2 - 2(m-n)\tilde{k})} \right] \\
&= \frac{1}{N} + \frac{2}{N} \sum_{\tilde{k}=1}^Q e^{i4\pi\frac{M}{N}\tilde{k}^2} \cos \left[ 4\pi\frac{\tilde{k}}{N}(m-n) \right].
\end{aligned} \tag{B1}$$

It is now seen that  $B$  is a symmetric matrix, i.e.,  $B_{m,n} = B_{n,m}$ .

- 
- [1] G. Casati, B.V. Chirikov, F.M. Izraelev, and J. Ford, in *Stochastic Behavior in Classical and Quantum Hamiltonian Systems*, edited by G. Casati and J.Ford, Lecture Notes in Physics, Vol. 93 (Springer, Berlin, 1979).
- [2] F. M. Izrailev, Phys. Rep. **196**, 299 (1990).
- [3] G. Lemarié, H. Lignier, D. Delande, P. Szriftgiser, and J. C. Garreau, Phys. Rev. Lett. 105, 090601 (2010); I. Talukdar, R. Shrestha, and G. S. Summy, Phys. Rev. Lett. 105, 054103 (2010); A. Ullah and M. D. Hoogerland, Phys. Rev. E 83, 046218 (2011); M. Lopez, J. F. Clement, P. Szriftgiser, J. C. Garreau, and D. Delande, Phys. Rev. Lett. 108, 095701 (2012); M. Sadgrove, T. Schell, K. Nakagawa, and S. Wimberger, Phys. Rev. A **87**, 013631

- (2013); B. Gadway, J. Reeves, L. Krinner, and D. Schneble, Phys. Rev. Lett. **110**, 190401 (2013).
- [4] S. Fishman, D.R. Grempel, and R.E. Prange, Phys. Rev. Lett. **49**, 509 (1982).
- [5] F. M. Izrailev and D.L. Shepelyansky, Theor. mat. Phys. **43**, 553 (1980).
- [6] P. Leboeuf, J. Kurchan, M. Feingold, and D. P. Arovos, Phys. Rev. Lett. **65**, 3076 (1990).
- [7] T. Geisel, R. Ketzmerick, and G. Petschel, Phys. Rev. Lett. **67**, 3635 (1991); R. Lima and D. Shepelyansky, *ibid* **67**, 1377 (1991).
- [8] R. Artuso, F. Borgonovi, I. Guarneri, and G. Casati, Phys. Rev. Lett. **69**, 3302 (1992); T. Prosen, I. I. Satija, N. Shah, Phys. Rev. Lett. **87**, 066601 (2001); I. I. Satija, Phys. Rev. E **71**, 056213 (2005).
- [9] G. M. Zaslavskii, M. Yu. Zakharov, R. Z. Sagdeev, D. A. Usikov and A. A. Chernikov, Sov. Phys. JETP **64**, 294 (1986).
- [10] I. Dana, Phys. Lett. A **197**, 413 (1995).
- [11] D. R. Hofstadter, Phys. Rev. B **14**, 2239 (1976).
- [12] J. Wang and J. B. Gong, Phys. Rev. A **77**, 031405(R) (2008).
- [13] P. H. Jones, M. M. Stocklin, G. Hur, and T. S. Monteiro, Phys. Rev. Lett. **93**, 223002 (2004).
- [14] I. Dana, E. Eisenberg, and N. Shnerb, Phys. Rev. E **54**, 5948 (1996).
- [15] J. B. Gong and J. Wang, Phys. Rev. E **76**, 036217 (2007).
- [16] To our knowledge, the smallest quasi-momentum spread in kicked-rotor experiments so far was achieved in the experiment reported in C. Ryu, M. .F. Andersen, A. Vaziri, M. B. d’Arcy, J. M. Grossman, K. Helmerson, and W. D. Phillips, Phys. Rev. Lett. **96**, 160403 (2006).
- [17] W. Lawton, A. S. Mouritzen, J. Wang, and J. B. Gong, J. Math. Phys. **50**, 032103 (2009); Note that the key result of this work is Eq. (42), which is clear only after referring to the proposition 29 detailed on page 23. Equation (42) itself is about the unitary equivalence between two extended versions of ORDKR and KHM after considering a union of their respective spectrum. Section III of the present work makes one step further by exposing a unitary equivalence under a certain parameter mapping without considering a spectral union.
- [18] I. Guarneri, *A note about double kicked rotors* (unpublished), 2008.
- [19] J. Wang, A. S. Mouritzen, and J. B. Gong, J. Mod. Opt.**56**, 722 (2009).
- [20] I. Dana, Phys. Rev. Lett. **73**, 1609 (1994); I. Dana and D. L. Dorofeev, Phys. Rev. E **72**, 046205 (2005); I. Dana, E. Eisenberg, and N. Shnerb, Phys. Rev. Lett. **74**, 686 (1995); I. Dana and



- D. L. Dorofeev, Phys. Rev. E **73**, 026206 (2006).
- [21] E. Tang, J. W. Mei, and X. G. Wen, Phys. Rev. Lett. **106**, 236802 (2011); K. Sun, Z. C. Gu, H. Katsura, and S. D. Sarma, Phys. Rev. Lett. **106**, 236803 (2011); T. Neupert, L. Santos, C. Chamon, and C. Mudry, Phys. Rev. Lett. **106**, 236804 (2011).
- [22] J. Wang, I. Guarneri, G. Casati, and J. B. Gong, Phys. Rev. Lett. **107**, 234104 (2011).
- [23] H. L. Wang, J. Wang, I. Guarneri, G. Casati, and J. B. Gong, Phys. Rev. E **88**, 052919 (2013).  
See also arXiv: 1308.3527.
- [24] D. Y. H. Ho and J. B. Gong, Phys. Rev. Lett. **109**, 010601 (2012). Note that in this reference, the eigenstates used to compute Chern numbers differ from those used here by a unitary transformation  $\exp[-i\hat{p}\varphi/(N\hbar)]$  that has no effect on the value of the Chern numbers.
- [25] T. Kitagawa, E. Berg, M. S. Rudner, and E. Demler, Phys. Rev. B **82**, 235114 (2010); N. H. Lindner, G. Refael, and V. Galitski, Nature Phys. **7**, 490 (2011).
- [26] I. Guarneri, Annals Henri Poincare **10**, 1097 (2009).
- [27] J. Wang and J. B. Gong, Phys. Rev. E **78**, 036219 (2008).
- [28] I. Dana, Phys. Rev. E **52**, 466 (1995); I. Dana, M. Feingold, and M. Wilkinson, Phys. Rev. Lett. **81**, 3124 (1998).